Journal Pre-proof

Metabolomic fingerprinting of renal disease progression in Bardet-Biedl syndrome reveals mitochondrial dysfunction in kidney tubular cells.

Emanuela Marchese, Marianna Caterino, Davide Viggiano, Armando Cevenini, Salvatore Tolone, Ludovico Docimo, Valentina Di Iorio, Francesca Del Vecchio Blanco, Roberta Fedele, Francesca Simonelli, Alessandra Perna, Vincenzo Nigro, Giovambattista Capasso, Margherita Ruoppolo, Miriam Zacchia

PII: S2589-0042(22)01502-4

DOI: https://doi.org/10.1016/j.isci.2022.105230

Reference: ISCI 105230

To appear in: *ISCIENCE*

Received Date: 22 July 2021

Revised Date: 28 February 2022

Accepted Date: 23 September 2022

Please cite this article as: Marchese, E., Caterino, M., Viggiano, D., Cevenini, A., Tolone, S., Docimo, L., Di Iorio, V., Del Vecchio Blanco, F., Fedele, R., Simonelli, F., Perna, A., Nigro, V., Capasso, G., Ruoppolo, M., Zacchia, M., Metabolomic fingerprinting of renal disease progression in Bardet-Biedl syndrome reveals mitochondrial dysfunction in kidney tubular cells., *ISCIENCE* (2022), doi: https://doi.org/10.1016/j.isci.2022.105230.

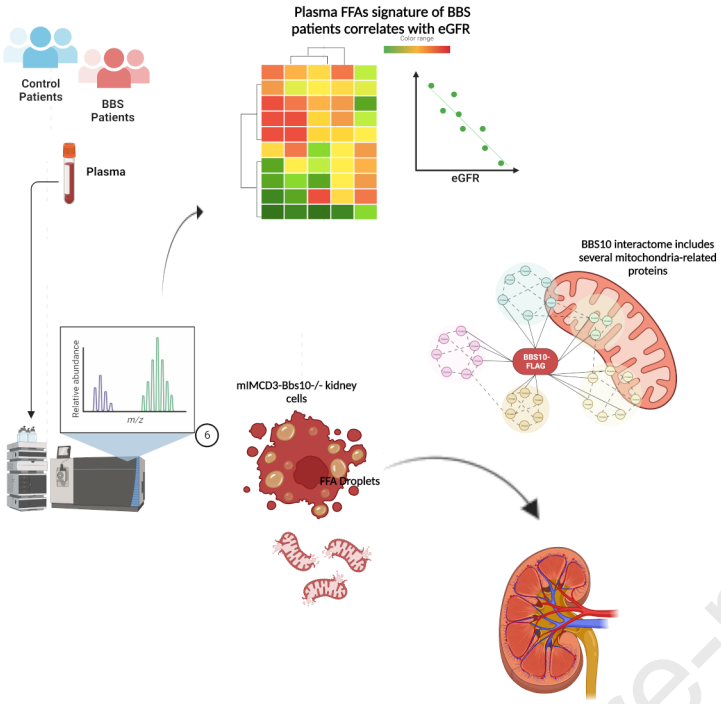

Metabolomic fingerprinting of renal disease progression in Bardet-Biedl syndrome reveals mitochondrial dysfunction in kidney tubular cells.

Emanuela Marchese[1,2], Marianna Caterino[2,3], Davide Viggiano[1,4#], Armando Cevenini[2,3], Salvatore Tolone[5], Ludovico Docimo[5], Valentina Di Iorio[6], Francesca Del Vecchio Blanco[7], Roberta Fedele[2], Francesca Simonelli[6], Alessandra Perna[1], Vincenzo Nigro[7], Giovambattista Capasso[4], Margherita Ruoppolo[2,3], Miriam Zacchia[1]

1. Dep. of Translational Medical Sciences, University of Campania “Luigi Vanvitelli”, Naples, Italy
2. Ceinge, Advanced Biotechnology, Naples, Italy
3. Dep. Molecular Medicine and Medical Biotechnology, University of Naples “Federico II”, Naples, Italy
4. Biogem, Ariano Irpino, Italy
5. Division of General, Mininvasive and Bariatric Surgery, University of Study of Campania "Luigi Vanvitelli", Naples, Italy
6. Eye Clinic, Multidisciplinary Department of Medical, Surgical and Dental Sciences, University of Campania "LuigiVanvitelli", Naples, Italy
7. Telethon Institute of Genetics and Medicine (TIGEM), University of Campania "Luigi Vanvitelli", Pozzuoli, Naples, Italy.

Corresponding authors:

Prof. Davide Viggiano

Prof. Giovambattista Capasso

Dep. of Translational Medical Sciences, University of Campania, “L. Vanvitelli”, via Pansini, 5 80131 - Naples, Italy

Tel/fax +39 081 566 6821; email: davide.viggiano@unicampania.it; gb.capasso@unicampania.i

Lead Contact

Prof. Davide Viggiano

Conflict of interest statement

The authors have declared that no conflict of interest exists.

Summary

Chronic kidney disease (CKD) is a major clinical sign of patients with Bardet-Biedl syndrome (BBS), especially in those carrying *BBS10* mutations.

Twenty-nine BBS patients and 30 controls underwent a serum targeted metabolomic analysis. *In vitro* studies were conducted in two kidney-derived epithelial cell lines, where *Bbs10* was stably deleted (IMCD3-*Bbs10*-/- cells) and over-expressed.

The CKD status affected plasmatic metabolites fingerprinting in both BBS patients and controls. Specific phosphatidylcholines and acylcarnitines discriminated eGFR decline only in BBS patients. IMCD3-*Bbs10*-/- cells displayed intracellular lipid accumulation, reduced mitochondrial potential membrane and citrate synthase staining. Mass-Spectrometry-based analysis revealed that human BBS10 interacted with six mitochondrial proteins, *in vitro.*

In conclusion, renal dysfunction correlated with abnormal phosphatidylcholines and acylcarnitines plasma levels in BBS patients; *in vitro, Bbs10* depletion caused mitochondrial defects while human BBS10 interacted with several mitochondria-related proteins, suggesting an unexplored role of this protein.

Introduction

Bardet-Biedl syndrome (BBS) is a rare inherited disorder characterized by multi-organ dysfunction. The phenotype of BBS patients is variable: the most common clinical findings include retinal dystrophy, obesity, polydactyly, intellectual disabilities and renal abnormality. The latter is characterized by a wide range of kidney and urinary tract malformations, including fetal lobulations, pelvic dilation, renal cysts, renal hypoplasia and vesical-ureteral reflux (Zacchia et al., 2016, Zaghloul and Katsanis, 2009). These structural anomalies are accompanied by functional defects, with a variable level of severity in available clinical studies, ranging from urine concentrating defect to the end stage renal disease (ESRD). The variability of kidney phenotype is at least in part dependent on the genetic heterogeneity of BBS; in fact, to date 24 genes have been defined as cause of human BBS and among these, *BBS10* is known to correlate with severe renal phenotype. The function of BBS proteins is only partially known; given their primary subcellular localization to the basal of the primary cilium (PC), the disorder is considered a ciliopathy.

There is significant evidence that energetic metabolism is impaired in both genetic and acquired kidney disorders (Zacchia et al., 2020, Zacchia et al., 2021b). Moreover, metabolomics has emerged as a valid tool to analyze metabolites within biological fluids, aiming at detecting disease-related biomarkers as well as molecular aberrations underlying pathologic conditions.

In this study, we characterize the serum metabolome profiling linked to renal disease in 29 BBS patients compared to a cohort of 30 controls, matched for age, gender, body mass index (BMI), and estimated glomerular filtration rate (eGFR). The control group included healthy volunteers and chronic kidney disease (CKD) patients suffering from glomerulonephritis and non-syndromic congenital anomalies of the renal and urinary tract (CAKUT). Our study revealed a clear separation of plasma metabolite profile of BBS patients with and without eGFR decline; moreover, a discrete group of metabolites appeared linked to the eGFR decline in BBS patients, indicating a BBS-specific effect.

The resulting BBS-specific metabolites linked to kidney damage included high molecular weight lipids of the classes of acylcarnitines (ACs) and phosphatidylcholines (PCs). ACs are intracellular molecules and PCs are cell membrane components and crucial signaling molecules. We tested if their precursors, long chain free fatty acids, were altered in tubular cells lacking Bbs10 gene. The deep investigation of lipid homeostasis alteration reveals that the reduction of *Bbs10* affects metabolic pathways, including mitochondrial dysfunction.

Finally, we showed that BBS10 protein interacts with six mitochondrial proteins, further suggesting its putative mitochondrial role and indicating a possible mechanistic explanation of kidney dysfunction in BBS.

Results

Patients

Twenty-nine adult patients with the clinical diagnosis of BBS according to Beales criteria (Beales et al., 1999) and 30 controls were enrolled. Features of patients and controls are listed in **Table 1**. Briefly, patients and controls included individuals with no differences in age, gender, max-Uosm, eGFR and BMI. To address whether changes in the eGFR affected plasma metabolites pattern, both BBS patients and controls were divided into two groups based on the eGFR. Specifically, BBS patients having an eGFR higher than 90 ml/min/1.73m^2 were referred as BBS with no chronic kidney disease (BBS_noCKD) while BBS patients having an eGFR lower than 90 ml/min/1.73m^2 were referred as BBS_CKD. Control subjects included healthy volunteers (ctr_hv) and subjects affected by CKD due to other causes (ctr_CKD), mainly glomerulonephritis and congenital anomalies of kidney and of urinary tract malformations (CAKUT). Genetic analysis (**Table 2**) of enrolled patients revealed that 9 patients showed mutations in chaperonin-like BBS proteins, with 6 and 3 patients bearing mutations in *BBS10* and *BBS12*, respectively; 3, 4 and 5 patients showed biallelic mutations in *BBS1*, *BBS4* and *BBS9*, respectively; one patient had two in trans *BBS2* mutations. Seven patients had no genetic diagnosis after molecular screening.

Metabolomic fingerprinting of CKD patients differed from non-CKD individuals, in both BBS patients and controls

A targeted metabolomic analysis was performed using serum samples from patients and controls, in order to quantify 180 metabolites (**Table S1 and S2**).

To identify the metabolites discriminating the CKD status (eGFR>90 vs eGFR<90 ml/min/1.73m^2) specifically in BBS patients we devised the following strategy: SPLS-DA, a supervised analysis of metabolome data, was used to discriminate the CKD state separately in the BBS and in non-BBS subjects. The results are presented in **Figure 1**. The PLS-DA algorithm optimally discriminated the CKD status based on metabolome data in both BBS and control populations (**Figures 1A-B**). ROC curves confirmed the high performance and robustness of the PLS-DA model (controls, AUC = 0.99; BBS patients, AUC = 0.94; **Figures 1C-D**). The relevance of each metabolite for the discrimination of the CKD status was identified by the Variable Importance in Projection (VIP) score (**Figures 1 E-F**). SPLS-DA allows for relevant feature selection and graphical displays for metabolomic data. The SPLS-DA output performance was tested using the receiver operating characteristic (ROC) curves.

Subsequently we computed the influence on the CKD categorization of every metabolite, retrieving the VIP.

VIP coefficients represent the importance of each metabolite to predict the CKD state. Metabolites with VIP score greater than 1 were then used for subsequent analysis. Therefore, two lists of metabolites with VIP score>1 were obtained, one for BBS patients and one for non-BBS patients. The two lists were then compared and only the metabolites present exclusively in BBS patients were then evaluated.

Variables with VIP score > 1 are shown in **Figure 2A** using a Venn diagram to display discriminating metabolites shared and unshared by the two populations (BBS controls). The list includes 29 metabolites shared among the two groups (25%). Shared molecules included biogenic amines, short chain acyl-carnitines and long-chain phosphatidylcholines.

We further filtered the list of BBS unshared metabolites using the following criteria: (i) metabolites not included in the list of controls VIP metabolites, (ii) presence of a significant correlation with the eGFR and (iii) presence of a significant difference between BBS and non-BBS regarding the calculated Pearson coefficient. The scatterplot of the eGFR vs the resulting 10 metabolites is presented in **Figure 2B** and **Table 2**.

We have further verified the effect of BBS and the connection with eGFR for these metabolites using a linear mixed model with the eGFR as dependent variable and (1) the metabolite concentration and (2) the BBS status (BBS vs controls) as predictors. All of the selected 10 metabolites show significant interaction metabolite concentration per BBS genotype (**Table 3**).

The resulting BBS-specific metabolites linked to kidney damage are high molecular weight lipids of the classes of acylcarnitines (ACs) and phosphatidylcholines (PCs).

Generation of inner medulla collecting duct (IMCD3)-Bbs10-/- model

The ACs are intracellular molecules and PCs are cell membrane components. We tested whether lipid metabolism is altered in tubular cells lacking Bbs10.

Figure 3A-B show the efficiency of Bbs10 invalidation, in IMCD3 cells. Real-time analysis of Bbs10 gene expression level in four independent clones of Bbs10-/- cells and wild type cells showed a dramatic decrease in *Bbs10* mRNA in mIMCD3 Bbs10-/- cells if compared with controls. The **Figures 3C-D** summarized the effect of *Bbs10* invalidation on the primary cilium (PC) formation: a dramatic reduction of ciliated cells was detected in IMCD3-Bbs10 -/- cells compared with the wild type. Moreover, Bbs10-/-cells showed a significantly increased mitotic rate compared with wild type cells (**Figure 3E)**.

IMCD3-Bbs10-/- cells showed increased cytosolic lipid droplets and signs of mitochondrial dysfunction

IMCD3-Bbs10-/-cells and controls were stained with oil red, after exposure for 24 hours to high FFA content medium. After treatment, IMCD3-Bbs10-/-cells showed an increased cytoplasmic accumulation of lipid droplets, suggesting an imbalance between lipid uptake and metabolism (**Figure 4A-C**). We therefore selected a series of enzymes to test mitochondrial dysfunctions in IMCD3-Bbs10-/-cells (Figure S1). Relative mRNA expression of CPT1, CPT2, ACOX1, PPAR alpha, PGC1a and PPAR gamma(H) was evaluated in experimental and wild type cells. The results didn't allow us to speculate about the observed alterations due to the low endogenous expression levels at basal in IMCD3 cells. Considering the role of mitochondria in the FFA metabolism, we studied overall mitochondria function in our cells. Immunofluorescence analysis revealed a significant reduction of mitochondrial membran potential (ΔΨM) in IMCD3-Bbs10 -/- cells compared to wild type cells, as showed by mitotracker CMXros fluorescence intensity (**Figure 5A-B**). Interestingly, experimental cells showed also a decreased citrate synthase (CS) staining (**Figure 5B**), a marker of intact mitocondria and total mitocondrial mass. In addition, protein amount of specific mitochondrial markers was tested (**Figure 5**). Finally, VDAC1, a marker of outer membrane mitochondria, resulted significantly increased in IMCD3-Bbs10 -/- cells compared to wild type cells (**Figure S1B**). To further validate the cellular model, we have analysed the presence of cellular inclusions using Red-oil staining in urine sediment of patients with BBS10 mutation. Results, shown in Supplementary figure S2 support the presence of lipids droplets in tubular cells of the urine sediment of BBS10 patients (see Supplementary figure S2 for details)

Protein-Protein interaction analysis revealed that BBS10 interactors included six mitocondrial proteins

In order to analyze the possibile link between mithocondrial dysfunction and Bbs10 depletion in cells, protein-protein interaction (PPI) studies were carried out, aiming at identify proteins that might interact with human BBS10. A cell line stably expressing BBS10-flag protein (HEK293T_BBS10) was generated. BBS10-flag protein was employed as baits in immunoprecipitation experiment (IP) in order to isolate and then identify its protein interactors. A cell line stably expressing GFP-flag protein was used as control. Interactome analyses identified BBS10 putative protein-ligands, by nano-LC-MS/MS and subsequent quantitative proteomic analysis (**Table S3**). Interstingly, six mitocondrial proteins were found among BBS10 interactors **(Table 4)**, including proteins involved in mitochondria biogenesis and function.

To estimate the BBS10-flag abundance compared to the endogenous protein, the amount of protein was measured in total extracts from HEK293T_BBS10 and wt HEK293T (HEK293T_CTRL) cell

lines by mass-spectrometry-based quantitative methods. The protein abundance was estimated by using normalized MS counts, as the ratio between the MS counts of the interest proteins and the total MS counts in the analyzed sample. According to normalized MS counts, the BBS10-flag abundance resulted 30-fold higher than endogenous protein (**Figure S3** and **Table S4**), while the levels of ACTB and TUBA proteins between the two samples were comparable.

Nuclear and mitochondrial localization of BBS10

Since PPI analysis identified six mitochondrial BBS10-interacting proteins (**Table 4**), we investigated if BBS10-flag protein localized in the mitochondria. To this aim, subcellular fractionation of cells stably expressing BBS10-flag protein was performed and a mitochondrial extract (MitoEx) was analyzed by western blot (WB) and compared with a whole cell extract (WCE) (Figure S4A). This analysis revealed that BBS10-flag might be present in the mitochondria, in a quite low abundance when compared to the WCE lane. The loaded amount of MitoEx and WCE corresponds to about the 13.7% and 6.4% of protein content from 10 million cells, respectively. The citrate synthase (CS) signal was used as a marker of mitochondrial fraction enrichment, while the complete absence of α-tubulin (TUBA) signal in the MitoEx lane demonstrate the complete absence of contamination from cytosolic fraction.

Among the BBS10 interactors, several nuclear proteins were identified. On the other hand, BBS10 protein is predicted to have a nuclear import motif and other BBS proteins are known to have also nuclear localization (Marchese et al., 2020). Immunoblotting studies of cytosolic (CytoEx) and nuclear (NuclEx) extracts revealed that BBS10-flag was also contained in the nuclei (Figure S4B). The histone H2 (H2AX) signal was used as a marker of nuclear fraction enrichment while a very faint band of α-tubulin (TUBA) in the NuclEx lane might indicate a very slight cytosolic contamination of the nuclei.

To further verify the localization of BBS10 protein in human renal tissue, three biopses from patients who underwent biopsy for proteinuria, but did not show significant modifications in the kidney structure, were studied. BBS10 protein was expressed in tubular cells at the level of the cytoplasm with minimal expression at nuclear level. Within the cytoplasm BBS10 has a diffuse staining pattern, with more intense spots that colocalized with MUT protein, a marker of mitochondria (**Figure S5**).

Discussion

The main result of the present study is the identification of a set of plasma metabolites linked to the presence of CKD selectively in BBS patients, along with evidence of a role of BBS10, one of major BBS locus, in mitochondrial activities/homoeostasis. We show that plasmatic metabolites discriminating BBS patients with CKD have high molecular weight and a lipophilic profile. Their precursors (long chain fatty acids) accumulate *in vitro* into kidney tubular cells lacking *Bbs10*, possibly because of impaired mitochondrial activities.

CKD is an important cause of morbidity and mortality in BBS patients. In this setting, kidney dysfunction is characterized by a wide range of severity, from urine concentrating defect to the end stage renal disease (Zacchia et al., 2016, Caterino et al., 2018, Zacchia et al., 2017). Little is known on the exact patho-mechanisms and no specific therapy is available. However, a recent meta-analysis showed that genetics may impact renal phenotype, demonstrating an association between *BBS10* mutations and severe renal phenotype in BBS patients. Our group has recently shown that urine concentrating defect is a presenting sign of kidney dysfunction, predicting eGFR decline and indicating the need of a more intensified monitoring (Zacchia et al., 2021a, Marchese et al., 2020).

The present study analyzes for the first-time plasma metabolic fingerprinting of patients suffering from BBS by using a targeted approach on plasma samples, a tool that has been shown to provide mechanistic insights underlying the pathogenesis of several disorders, including kidney diseases(Liu et al., 2010).

The study revealed a clear separation of plasma metabolite profile of BBS patients with and without eGFR decline; similar results were obtained in a control group, including healthy subjects and CKD due to other causes. Interestingly, several molecules discriminating individuals with declined eGFR were shared among BBS and controls, suggesting that CKD strongly affected metabolic plasma composition. The VIP metabolites shared between BBS patients and controls are known to be associated with CKD and are included in the group of molecules known as uremic toxins (Perna et al., 2019, Perna et al., 2016).

At variance, 10 metabolites appeared linked to the eGFR decline only in BBS patients, indicating a BBS-specific effect. These metabolites have high molecular weight, a lipophilic physical property and include several phosphatidylcholines and acylcarnitines. Unfortunately, given the high genetic heterogeneity of our BBS cohort, the study is not powered enough to show possible correlations between metabolites and specific genotypes; thus, the analysis was conducted in the entire BBS cohort and the results were compared with non-BBS individuals.

As plasmatic phosphatidylcholines are major components of plasma lipoproteins, one possible explanation is that abnormal phosphatidylcholines plasma levels reflect dyslipidemia, a common

finding in BBS patients. This hypothesis required further analysis. The specific relationship of three acylcarnitines with the eGFR in BBS patients attracted our attention.

Carnitine and its esters are detected in all biological fluids, including the plasma. As long-chain-fatty-acid are impermeable to mitochondrial membranes, carnitine serves as shuttle for their transport to the mitochondria (Costanzo et al., 2017).

The kidneys are highly metabolic organs which use high levels of ATP to exert its functions, especially tubular reabsorption. Mitochondrial fatty acid oxidation (FAO) serves as the preferred source of energy production (Liu et al., 2010, Zacchia et al., 2018). The excess of fatty acids that are not catabolized by mitochondria are esterified with glycerol and deposited as lipid droplets. To shed light into abnormal acylcarnitine levels in BBS patients with kidney impairment, we used an *in vitro* model of BBS, renal-derived epithelial cell line (IMCD3) lacking *Bbs10*, as the latter is one of major BBS genes correlating with kidney dysfunction in BBS patients, according to the literature (21). The model was developed using the CRISP/CAS9 approach, which allowed a dramatic reduction of *Bbs10* genetic transcription; unfortunately, the low endogenous Bbs10 protein abundance in IMCD3 cells hindered its quantification in both wild type and depleted cells, at protein levels. However, our results showed that experimental cells displayed metabolic aberrations, characterized by intracellular lipid accumulation and mitochondrial dysfunction. To further validate the cellular model, we have analyzed the presence of cellular inclusions using Red-oil staining in urine sediment of patients with BBS10 mutation. Our results support the presence of lipids droplets in tubular cells of the urine sediment of BBS10 patients.

Increased lipid accumulation is well described in several experimental models of nephropathies, including acquired metabolic kidney disorders (obesity and diabetic nephropathy), acute and chronic kidney disease and even genetic disorders (Thongnak et al., 2020). It is debated whether lipid accumulation is the cause or the result of kidney injury. It is believed that increased intracellular lipid deposit is the effect of an imbalance between lipid production/uptake and lipid catabolism. Altered mitochondrial function is considered a cause of renal lipid drops accumulation in diabetic nephropathy.

We found sings of mitochondrial dysfunction in IMCD3 cells lacking *Bbs10*, as shown by reduced potential membrane and citrate synthase staining.

Whether mitochondrial dysfunction may be the cause or the effect of lipotoxicity was unclear. However, we performed the analysis of BBS10 interactors, using a functional proteomics approach, to provide further insights into the link between Bbs10 depletion, lipid cellular accumulation and mitochondrial dysfunction. Interestingly, we found that BBS10 interactors, *in vitro*, included six mitochondrial proteins. It's intriguing to note the known BBS10 interactors, BBS6 and BBS12, were

not found in our analysis. Unfortunatelly, mass spectrometry methods were unable to detect poorly abundant proteins and/or ligands weakly interacting with BBS10. In fact, the interaction between chaperonin-like BBS proteins has been demonstrated by alternative methods (Seo et al., 2010).

The interaction of BBS10 with several mitochondrial proteins prompted us to better analyze its subcellular localization. For the first time, we showed that in HEK cells over-expressing human BBS10, the protein localizes in all cellular compartments, cytoplasm, nucleus and mitochondria. To corroborate this finding, we studied BBS10 protein levels in renal biopsy samples of individuals with proteinuria, that did not show significant abnormalities in kidney structure. BBS10 protein was detected in tubular cells; within the cytoplasm it showed a colocalized with a marker of mitochondria, confirming in humans its extra-basal body localization. However, BBS10 has no known target sequence to mitochondria, according to DeepMito software. Therefore, the molecular interaction of BBS10 and the mitochondrial proteins found by immune-preciptiation must be interpreted with caution. Since immunoprecipitation destroys the subcellular localization of proteins, BBS10 might artificially arrive in contact with proteins that would be sequestered in subcellular compartments. Among the interactors described in **Table 4**, the BAG2 protein is expressed on the outer mitochondrial membrane and therefore might physically interact with BBS10.

As stated above, the link between mitochondrial dysfunction and CKD is an intriguing and emerging paradigm (Bhatia et al., 2020). In the last years, the phosphatase and tensin homolog (PTEN)-induced kinase 1 (PINK1) and PARKIN have been shown to participate to a signalling pathway governing mitochondrial quality control (Valente et al., 2004, O'Flanagan and O'Neill, 2014). The PINK1/Parkin signaling activates ubiquitination of outer mitochondrial membrane proteins to promote priming dysfunctional mitochondria for lysosome degradation pathways. Interestingly, Bcl2-associated athanogene 2 (BAG2), one of BBS10 interactors in our study, was identified as a mediator promoting mitophagy by inhibiting PINK1 ubiquitination and degradation (Luciani et al., 2020) (Qu et al., 2015). The role of BBS10-BAG2 interaction is not known; if BBS10 is required for correct BAG2 function, we could expect abnormalities in cleaning cells from damaged mitochondria. Our findings showed a decreased mitochondrial membrane potential in cells lacking Bbs10. Moreover, immunoblotting studies revealed an increased abundance of Vdac1 compared to control cells. Our data suggest that *Bbs10* deficiency may lead to cellular accumulation of dysfunctional mitochondria (**Figure 6**).

Even though the exact link between mitochondrial dysfunction/increased intracellular lipid accumulation/and kidney impairment should be better deciphered, as well as the direct role of BBS10 depletion in mitochondrial clearance, this study shows for the first time that CKD in BBS patients is characterized by metabolic abnormalities, including both common features of CKD and specific BBS

abnormalities; these alterations could be the result of a specific role of BBS proteins on renal epithelial mitochondrial homeostasis, at least in the setting of Bbs10 depletion.

Limitation of study

The study has some limitations. The patients' cohort is quite heterogenous at genetic levels: the selection of *BBS10*-mutated patients would reduce patients' number, affecting the statistic power of our analysis. Moreover, CRISPR/Cas9 technology brings its own limitation, including the difficulty to exclude off-target effects. Future experiments might also take into consideration rescue experiments, which are exceedingly difficult in this cellular model. Finally, further studies are needed to elucidate the exact mechanisms linking *Bbs10* invalidation/mitochondrial abnormalities/BBS10 interaction with mitochondria-related proteins.

Star Methods

Key resource table

Materials	Ca.no	Vendor
FlexiGene DNA Kit (250)	51206	Qiagen
AbsoluteIDQ® p180 kit	0073.6	Biocrates Life Science
Bbs10 CRISPR/Cas9 KO Plasmid (m)	Sc-428052	Santa Cruz
Bbs10 HDR plasmid (m)	Sc-428052-HDR	Santa Cruz
Control CRISPR/Cas9 Plasmid	sc-418922	Santa Cruz
BBS10 cDNA ORF Clone, Human, N-DYKDDDDK (Flag®) tag	HG29785-NF	Sino Biological
Lipofectamine 2000	11668030	Thermo Fisher Scientific
Oil Red O powder	Cod. O-0625	Sigma-Aldrich
Mitotracker Red CMXRos	M7512	Thermo Fisher Scientific
Mowiol 4-88 Reagent	475904100GM	MilliporeSigma
Arl13b	17711-1-AP	Proteintech
γ-tubulin	T6557	Sigma-Aldrich
S-Trap™ micro	N\A	Protifi
Anti-FLAG® M2 Magnetic Beads	M8823	Sigma-Aldrich
3X FLAG® Peptide	F4799	Sigma-Aldrich
EUROGOLD TriFast	961590054	EuroClone
SuperScript™ VILO™ MasterMix	11756050	Thermo Fisher Scientific
Qproteome Cell Compartment Kit	37502	Qiagen
Citrate synthase	ab96600	Abcam
Tubulin	T6074	Sigma-Aldrich
Flag M2	F1804	Sigma-Aldrich
Vdac1	AB10527	Millipore

Resource availability

Lead contact

The raw data and other study materials will be provided after request to the corresponding author, Prof. D. Viggiano.

Materials availability

This study did not generate new and unique reagents.

Data and code availability

Data used in statistical analyses have been deposited in the paper's supplemental information and are available as of the date of publication.

All original codes are available in the paper's supplemental information.

Any additional information required to reanalyze the data reported in this paper is available from the lead contact upon request.

Experimental model and subject details

Subject enrollment

Patients referring to the ambulatories of rare kidney and ocular disorders of the University of Campania, L.Vanvitelli with a clinical diagnosis of BBS according to Beales criteria (Beales et al., 1999) were enrolled in the study. Kidney function was evaluated estimating the GFR (eGFR) using the CKD-Epidemiology Collaboration Equation (CKD-EPI), which considers serum creatinine levels, age, gender and race (Levey et al., 2009). Given the young age of patients, chronic kidney disease (CKD) was defined as an eGFR lower than 90 ml/min/1.73m^2. Post-axial polydactyly was defined as the presence of an extra-finger; retinal dystrophy was assessed after ocular examination; obesity was defined as body max index over 30 Kg/m^2. Intellectual disability referred to defect in writing, spelling, speaking or memories /social/coordination defects.

Clinical (age, gender, comorbidities) and anthropometric parameters (height, weight and body mass index) were investigated at basal visit.

Renal function was assessed as follows: the glomerular filtration rate (eGFR) was estimated using CKD-EPI formula or Schwarts formula in children (<15years). Serum creatinine was measured with an enzymatic method on an autoanalyzer, and the values were rounded to the second decimal point. Maximal urine concentration ability was assessed on second void urine sample, collected after over 12h fasting and dehydration; urine osmolality was measured by a freezing point depression osmometer (model 3320 osmometer, Advanced Instruments, Inc.) as detailed elsewhere(Caterino et al., 2018, Zacchia et al., 2016).

Study approval

This study is in full compliance with the Declaration of Helsinki. Human studies have been approved by the Institutional Review Boards of the University of Campania L. Vanvitelli (N 76, 24/02/2014). Written informed consent was received from participants prior to inclusion in the study. Participants have been identified by number, not by name.

Method details

Genetic Analysis

All patients underwent genetic analysis using Next Generation Sequencing (NGS) technology. Written informed consent was obtained from all participants; genomic DNA was extracted from whole blood sample with the FlexiGene DNA Kit (Qiagen) following the manufacture'instruction. Patient DNA analysis by NGS was performed with the Illumina MiSeq System, as described previously (20). The variant frequency was analyzed with the ExAC database and *in silico* prediction tools, including Polyphen and SIFT, were used to assess pathogenicity. Putative pathogenic variants were confirmed by Sanger sequencing (3130 Genetic Analyzer Applied Biosystems), according to the manufacturer's protocol. Genotype-phenotype analysis was elucidated after consultation of specific Databases as Pubmed, ClinVar and OMIM. Each new variant was analyzed for inheritance and parental segregation.

Serum collection and preparation

Blood samples were obtained after an overnight fast. Blood was centrifuged (10 minutes, 2000 g at 4°C) and plasma was aliquoted into separate polypropylene tubes that were immediately stored at -80°C. One 10-µL aliquot was analyzed with the Biocrates AbsoluteIDQ p180 kit (Biocrates Life Science AG, Innsbruck, Austria), as recommended by the manufacturer and analyzed on a Triple Quad™ 5500+ System QTrap-Ready (AB Sciex) coupled with an Agilent 1260 Infinity II HPLC equipped with an Agilent C18 HPLC column.

Targeted metabolites identification and quantification

The Biocrates AbsoluteIDQ p180 kit ((BIOCRATES Life Sciences AG, Innsbruck, Austria) is a mass spectrometry-based metabolome platform that allows the identification and quantification more than 180 metabolites, combining a flow injection analysis (FIA) and a liquid chromatography (LC) method. It allows to measure metabolite, including amino acids, biogenic amines, acylcarnitines, lysophosphatidylcholines, phosphatidylcholines, sphingomyelins and the sum of hexoses (one resultant metabolite) (Caterino et al., 2021, Imperlini et al., 2016). Serum sample preparation was carried out according to the manufacturer’s protocol (Biocrates, User Manual-P180). Briefly, 10 µL of sample (serum sample, quality controls, zero samples, or calibrators) were added onto the filter inserts and dried for 30 min under a nitrogen stream. Quantification was carried out using internal standards (ISTD) and a calibration curve (Cal 1 to Cal 7). Three human plasma samples spiked with

different concentrations of reference analytes (QC1-3) were analyzed as quality control, according to manufacturer's protocol. Metabolites and their abbreviations were summarized in **Table S1**. Amino acids and biogenic amines were derivatized for 20 min with an excess of 5% phenylisothiocyanate in ethanol/water/pyridine (ratio 1/1/1, v/v/v), and subsequently dried for 45 min under a nitrogen stream. Metabolites and internal standards were then extracted with 300 µL methanol containing 5 mM ammonium acetate by shaking for 30 min and eluted by centrifugation for 5 min at room temperature and 450 rpm. From the eluate 50 µl was diluted with 450 µl of 40% methanol (50/50, v/v in HPLC grade water) for the LC-MS/MS analysis, and 10 µl of the eluate was diluted with 490 µl of FIA kits' running solvent (1/5, v/v) for the FIA run.

For the FIA analysis the injection volume was 20 µL with a solvent mobile at an initial flow rate of 0.03 ml/min until 1.6 min, followed by 0.20 ml/min for 1.6 min and 0.02 ml/min for 0.20 min. The auto sampler was cooled at 10 °C. The ion source was operated in positive ion mode using the following parameters: spray voltage 55 kV, temperature of 450 °C, GS1 20, GS2 40, CUR 30, CAD 8. The ion source was operated in negative ion mode using the following parameters: spray voltage 55 kV, temperature of 450 °C, GS1 20, GS2 40, CUR 30, CAD 8. Data were acquired using Analyst software (version 1.7 Ab Sciex) and Concentrations of metabolites monitored by FIA were directly calculated in MetIDQ™ Oxygen 2976 (Biocrates Life Sciences Innsbruck, Austria).

Evaporation steps were performed using a nitrogen evaporator (Ultravap, Porvair Sciences, Leatherhead, Great Britain), and mass spectrometry analyses were done on using on a Triple Quad™ 5500+ System QTrap-Ready (AB Sciex) coupled with an Agilent 1260 Infinity II HPLC and controlled by the Analyst 1.7 software (ABSciex). Liquid chromatography was performed on a C18 column (Zorbax eclipse XDB 3 × 100 mm, 3.5 µm) using acetonitrile and water with 0.2% formic acid as running solvent. FIA-MS analyses was performed by using FIA kits' running solvent as the running solvent. Finally, the molecular species quantification was carried out by MRM, Multiple Reaction Monitoring).

On each plate, three plasma samples spiked with different concentrations of reference analytes (QC1-3) and five reference plasma samples (human plasma) were run to serve as quality control and for the evaluation of plate effects, respectively. For each of the three extraction solvents, 10 µL of solvent were transferred three times onto the kit plate and analyzed with internal standards serving as zero samples. Metabolites' concentrations were summarized in **Table S2**.

Generation of a cell line lacking *Bbs10* using CRISPR/Cas9 technology

To obtain mIMCD3 with *Bbs10* gene knockout we used by the CRISPR/Cas9 technique as previously described (Costanzo et al., 2020a). Two types of plasmidic constructs (Santa Cruz Biotechnology)

were used: i) Bbs10 CRISPR/Cas9 KO Plasmid (m) and ii) Bbs10 HDR plasmid (m). The first type of construct is able to transiently express Cas9 nuclease and a single guide RNA (sgRNA) directed to an exon in the 5' region of murine Bbs10 gene. Indeed, the Bbs10 CRISPR/Cas9 KO Plasmid (m) consists of a pool of three different plasmids which differ each other only for a sequence of 20 nucleotides of the sgRNA. In fact, each of three sgRNA is directed to a different site (Figure S6) in the 5' region of the Bbs10 gene. Therefore, the three sgRNAs and Cas9 generate three different double strand break (DSB) sites in the Bbs10 gene.

The second type of construct [Bbs10 HDR plasmid (m)] contains two regions which are called Arms and which have sequences that are totally homologue to the regions flanking the DSB. When Cas9 generates the DSB, the presence of HDR plasmid enable the Homology-directed Repair (HDR) and the Arms are used by the cell as DNA template for this process. The Arm that maps upstream [on the sense (+) strand] the DSB site is called 5' Arm, while the Arm that maps downstream the DSB site is called 3' Arm (Figure S5). Among the two Arms there is an expression cassette able to express a red fluorescent protein (RFP) and a gene which confers resistance to puromycin (Puro). Therefore, the effect of the HDR process is the insertion of such expression cassette within the DSB site. Thus, the cell clones with Bbs10 KO produce RFP and are resistant to puromycin. Since three different sgRNAs are used to generate as many DSBs, also the Bbs10 HDR plasmid (m) consists of a pool of three different plasmids which differ each other for the sequences of the Arm pairs. Each Arm pair is designed to flank one corresponding DSB site. Briefly, 1.5×10^3 cells/mm^2 of wild type cells were seeded in a 10 cm diameter plate with culture medium without antibiotics. After 24 h, the cells were transfected using Lipofectamine 2000 (Thermo Fisher Scientific, Waltham, MA, USA) as transfection reagent. 48 h after the transfection, the cells were incubated in a selective medium containing 3 µg/mL puromycin (Santa Cruz Biotechnology, Dallas, TX, USA). The culture of transfected cell (*Bbs10* -KO pool) was kept in the selective medium for several days with two-day changes of medium to eliminate detached cells and to preserve adherent puromycin-resistant cells. In the following weeks, the puromycin-resistant cells were detached, and re-plated after a proper dilution, in order to have separate colonies, each one deriving from a single resistant cell clone. RFP signal was used as a marker of the efficiency of the CRISPR/Cas9-mediated genome-editing. The colonies with a brighter RFP signal were then detached and kept in culture separately. *Bbs10* -KO pool and the clones (four *Bbs10* KO) were tested by qRT-PCR, in order to confirm the *Bbs10* deletion. To consider possible off-target effects of CRISPR-CAS 9 BBS10 deletion, we have exploited three guide RNAs which bind to three different sites within the same BBS10 gene (homology-directed repair, HDR). This strategy increases the efficiency of the deletion and its accuracy (see Supplementary Figure S5). Furthermore, this construct has been inserted in three different cell

mIMCD3 clones with different DNA insertion sites. Therefore, any off-target effect of CRISPR-CAS 9 insertion would be expected to have low chance to appear in all four clones. Control cells consisted in mIMCD3 cells transfected with Cas9 Nuclease Only. To limit clone dependent effects, four different KO clone cells were used, in addition to the negative control line transfected with Cas Nuclease Only".

Generation of a cell line stably expressing BBS10 for protein-protein interactions (PPIs).

For the generation of cell line stably expressing BBS10-flag protein, 1.5 × 103 cells/mm2 of Hek293t/17 wild type cells were seeded in a 10 cm diameter plate and kept in culture in a medium without antibiotics. After 24 h, cells were transfected by using 10 µg of BBS10 cDNA ORF Clone, Human, N-DDK (Flag) tag expression plasmid (Sino Biological, SB) and Lipofectamine 2000 (Thermo Fisher Scientific, Waltham, MA, USA) following the supplier instructions. 48 h after the transfection, the cells were incubated in a selective medium containing 75 µg/mL hygromycin (Santa Cruz Biotechnology, Dallas, TX, USA). The culture of transfected cell (BBS10-flag pool) was kept in the selective medium for several days with two-day changes of medium to eliminate detached cells and re-plated after a proper dilution, in order to have separate colonies, each one deriving from a single resistant cell clone. The colonies were then kept in culture separately. BBS10-flag pool and the clones were tested by WB to verify the presence of flag tagged protein expression.

Lipids Oil Red O Staining

Bbs10 depleted cells and wild type cells were treated with a mixture of Palmitic and oleic acid to a final concentration of 1nM for 24 hours. Before treatment, lipids were dissolved in ethanol and coniugated with 10 % BSA.

Cell Fixing: media was removed from cells and cells were gently washed twice with PBS. Paraformaldehyde (PFA, 4%) was added to each well and incubated for 30 min to 1 hr.

FFA uptake was demonstrated by Oli Red O staining (red). Nuclei were counterstained with Hematoxylin (blue). To this aim PFA was removed and cells washed as needed with dH2O. Isopropanol (60%) was added to each well and incubate for 5 min. Oil red stock solution was prepared dissolving 60 mg of Oil Red O powder (sigma cod. O-0625) in 20 ml of of 100% isopropanol. To make Oil Red O Working Solution, add 3 parts of Oil Red O Stock Solution to 2 parts of dH2O, mix well. Oil Red O Working Solution was then filtered with 0.2 µm syringe filter and ready to use.

At this point, Isopropanol was discarded and replaced with Oil Red O Working Solution (sigma). Cells were incubated for 10-20 min. Oil Red O solution was kept out and cells were wash 2-5X with dH2O as needed until excess stain is no longer apparent. At the end Hematoxylin was added to cells for nuclei staining and incubated for 1 min. Hematoxylin was removed and the cells were again washed dH2O and the microscopy slides were mounted for detection with Mowiol 4-88 Reagent

(Millipore, Billerica MA, Usa cod. 475904). Under microscope, lipid droplets appear red and nuclei appear blue.

The amount of FFA droplets were quantified by three blinded independent observers who were instructed to give a score from 0 (no cells with droplets) to 2 (all cells showing droplets). For each condition the average score among blinded observers was considered. The resulting average scores in experimental triplicates were then statistically analyzed using ANOVA and planned comparisons with Student's t-test.

Mitochondrial membrane potential

Cells were seeded at a density of 2x 10^3 cells/mm^2 in a 24-well plate. After 24 h, cells were stained with Mitotracker CMX-ROS (Ex/Em: 579/599) which accumulates in active (healthy) mitochondria with intact membrane potentials. Mitotracker CMX-ROS (200nM) solution was pre-warm before incubating with cells for 40 min at 37°C. Cells then were washed twice in PBS and fixed in cold methanol for 10 min. Blocking was performed in PBS 0.1% TritonX-100 with Fetal Serum Bovine (FBS) at final concentration of 5%. Cells were incubated with primary antibody against Citrate synthase (ab96600, Abcam) over night at 4°C. Bound antibody were detected with 488 Alexa-Fluor-conjugated donkey anti-rabbit IgG antibody (Life Technologies). After two additional washes in PBS 0.1% TritonX-100, cells were incubated with a solution of 300 nM DAPI (Thermo Fisher Scientific, Waltham, MA, USA) in PBS for 10 min. The cells were again washed twice with PBS and the microscopy slides were mounted for detection with Mowiol 4-88 Reagent (Millipore, Billerica MA, USA cod. 475904). Mitochondrial images were acquired with the confocal microscope LSM980 with 63X objective (NA 1.4) using Airyscan detector. Laser wavelength: 405, 488, 561 nm. Quantification of cell area (µm^2) and fluorescence intensity was performed using Zen 3.1 software.

Cilia staining and BBS10 staining in human kidney biopsies

After 48 h from seeding, the cells were starved in 0.1% of FBS medium to induce ciliogenesis. Cilia staining was performed after 24 h and 48 h from starvation, respectively. Cells were than washed twice with PBS and fixed in cold methanol for 10 min. Blocking was performed in 1X PBS, 0.1% of saponin, 0.75% of BSA, 50mM ClNH4. The primary antibodies Arl13b (17711-1-AP, Proteintech) and γ-tubulin (T6557 Sigma) were diluted in the blocking solution and incubated over night at 4°C. The secondary antibodies (488 Alexa Fluor and 594 Alexa Fluor, Thermo Fisher Scientific) were incubated for 1 h at room temperature. After two additional washes in PBS 0.1% TritonX-100, cells were incubated with a solution of 300 nM DAPI (Thermo Fisher Scientific, Waltham, MA, USA) in PBS for 10 min. The cells were again washed twice with PBS and The microscopy slides were mounted for detection with Mowiol 4-88 Reagent (Millipore, Billerica MA, Usa cod. 475904). Z stack were first acquired with Cell Discoverer7(9 slices-2.72µm), using Plan –Apochromat 20/0.95

objective and 2x tubulens optovar, to obtain high content images for quantification of cilia number. Automated analysis was performed with Zeiss Zen Intellesis module of Zen blue 3.1. Cilia count was normalized for numbers of cellular nuclei. Then, for each sample, 3 representative fields were acquired with confocal microscope LSM980 using 63X objective (NA 1.4) and Airyscan detector in order to obtain high resolution images. All results shown are representative of at least 3 independent experiments.

To analyse the colocalization of BBS10 and mitochondria in the kidney tubules, we performed immunofluorescence on kidney criosections from kidney biopsies of (non-BBS) patients that did not show significant changes in the kidney structure. Three biopsies were analyzed without significant qualitative changes among patients. For this experiment we used a double immunofluorescence staining against BBS10 (rabbit polyclonal 1:100) and methylmalonyl-CoA mutase (MUT, mouse monoclonal 1:100). The specificity of the anti-BBS10 antibody has been tested by western blot as reported in a previous published work (29). Primary antibodies were then visualized using anti-rabbit-Alexa 488 (green fluorescence) and anti-mouse-Alexa 594 (red fluorescence) respectively. DAPI was used as nuclear counterstaining. Sections were analyzed with a Zeiss Confocal microscope LSM 980 coupled with Airyscan module.

Immunoprecipitation

Lysis Buffer: 1X TBS (250 mM Tris-HCl pH 7.4, 1.40 M NaCl, 0.03 M KCl) 1mM EDTA, 1% Triton X-100, 10 % glycerol, proteinase inhibitors. Washing Buffer: 1X TBS (250 mM Tris-HCl pH 7.4, 1.40 M NaCl, 0.03 M KCl) 1mM EDTA, 10 % glycerol, proteinase inhibitors. HEK293 cells expressing BBS10-flag and the GFP-flag vector used as control were lysate with the Lysis Buffer. Total protein extracts were pre-cleared with mouse IgG agarose beads and incubated ON at 4 °C with M2 anti-FLAG agarose-conjugated antibody beads (Sigma). The control experiment obtained by immunoprecipitation of GFP-flag vector transfected cells with anti-FLAG agarose beads allowed to rule out unspecific retained proteins as described. Non-retained proteins were then incubated with M2 anti-FLAG agarose-conjugated antibody beads (Sigma) overnight at 4 °C. Beads were washed with washing Buffer. Retained protein complexes were eluted with 3XFLAG peptide and subjected to precipitation with methanol/chloroform. The protein mixture was vacuum-dried and re-suspended in 10% SDS buffer to perform *in situ* protein hydrolysis with S-TrapTM micro spin column for interactors identification.

Interactome analysis

The protein extract from HEK293T_BBS10 and wt HEK293T (HEK293T_CTRL) cell lines or immunoprecipitated samples (IP) were resuspended in 10% SDS buffer. The samples were then reduced in 100 mM TCEP (Sigma-Aldrich, St. Louis, MO, USA) and carbamidomethylated in 50

mM iodoacetamide (Sigma-Aldrich, St. Louis, MO, USA) (Caterino et al., 2014). Aqueous phosphoric acid was added to a final concentration of 1.2%. A six-time volume of S-Trap buffer (90% aqueous methanol, 100 mM TEAB, pH 7.1) was added to protein complex. Finally, the mixtures were put on the S-Trap micro columns and centrifuged at 4000× g for 30 s. Three washes were carried out by using 150 µL S-Trap binding buffer. The mixtures were digested using 3µg of trypsin (Promega) at 47°C for 1h. After elution, peptides were vacuum dried down and resuspended in 35 µL of 10% ACN, 0.1% TFA in HPLC-grade water prior MS analysis.

nanoLC-MS/MS Measurements

NanoLC-MS/MS analysis was carried out in order to process tryptic peptide mixtures from: i) extracts from HEK293T_BBS10 and wt HEK293T (HEK293T_CTRL) cell lines; ii) four independent biological replicates of BBS10-flag IP and four replicates for GFP-flag IP (Costanzo et al., 2018, Costanzo et al., 2020b). Samples were resuspended in 100 µL of 10% ACN, 0.1% TFA in HPLC-grade water. For each run, 5 µL were injected in a nanoRSLC-Q Exactive PLUS (RSLC Ultimate 3000) (Thermo Scientific, Waltham MA, USA). Peptides were loaded onto a µ-precolumn (Acclaim PepMap 100 C18, cartridge, 300 µm i.d.×5 mm, 5 µm) (Thermo Scientific), and were separated on a 50 cm reversed-phase liquid chromatographic column (0.075 mm ID, Acclaim PepMap 100, C18, 2 µm) (Thermo Fisher Scientific). Chromatography solvents were (A) 0.1% formic acid in water, and (B) 80% acetonitrile, 0.08% formic acid. Peptides were eluted from the column with the following gradient 5% to 40% B (120 minutes), 40% to 80% (1 minutes). At 121 minutes, the gradient stayed at 80% for 5 minutes and, at 127 minutes, it returned to 5% to re-equilibrate the column for 20 minutes before the next injection. Eluting peptide cations were ionized and analyzed using a Q Exactive PLUS mass spectrometer (Thermo Scientific, Waltham MA, USA). Tandem MS was performed by data-dependent acquisition (DDA) and the top 10 intensity precursor ions were fragmented by higher-energy collisional dissociation (HCD). The MS scan range was from 400 to 2000 m/z. The mass spectrometry parameters were set as follow in MS and MSMS scan: resolution 70,000 and 17,500; AGC (automatic gain control) target 3.10^6 and 1.10^5 counts; maximum injection time 200 and 120 ms in MS and MSMS respectively.

Mass Spectrometry raw-files data processing

Raw data were processed using MaxQuant software version 1.6.5.0 and searched against Homo sapiens database (Swiss-Prot 07/2017) by Andromeda search engine. Mass Error Tolerance were set to 4.5 ppm and 20 ppm for precursors and fragments, respectively. Additional search parameters: enzyme specificity: trypsin; enzyme missed cleavages: two per peptide; fixed modification: cysteines carbamidomethylation; variable modification: methionines oxidation, N-term acetylation. Match between runs was not allowed. The false discovery rates (FDRs) threshold lower than 1%. on peptides

and proteins. The reverse and common contaminants hits were removed from total output identified protein list. Proteins were quantified using MS1 peak intensity (LFQ, label free quantification value) as quantitative parameters, according to the MaxQuant label-free algorithm.

The proteome datasets of BBS10-flag and GFP-flag interactomes were analyzed with the Perseus software version 1.6.0.7 (www.perseusframework.org, MPI of Biochemistry, Martinsried, Germany). The identify BBS10 interactors purified by immunoprecipitation the following strategy was used: 1) imputation of undetectable peptides: peptides whose expression level was below the detection threshold of the method were considered having a value corresponding to the lowest LFQ intensity (among all peptides) observed in that experiment. 2) repeated t-tests were performed for each interactor, comparing the control cells (expressing only GFP-Flag) and BBS-10-Flag cells 3) to take into account the statistical effect of repeated t-tests, the False Discovery Rate (FDR) was calculated using the function p.adjust (method="fdr") in R environment. 4) Only interactors with FDR>0.05 were then considered 5) we have additionally selected candidate interactors on the basis of the effect size, by including only changes in expression level, Δ (LFQ controls - LFQ BBS10_flag), lower than 1.4. The details of mass spectrometry protein identification and quantitation of BBS10 putative interactors are listed in supplementary **Table S3**.

In supplementary **Table S3**, for each identified protein in the immunoprecipitated fraction the following parameters are reported:

1. The identification codes, as Gene names, Protein IDs, and Protein names
2. The mass spectrometry quantitative parameters, as LFQ (Label Free quantification) for each biological replicate of the two conditions (CTRL and BBS 10)
3. The mass spectrometry identification parameters, as Unique peptides (number peptides), Unique sequence coverage (protein sequence coverage, calculated according to the number of peptides identified for each protein), molecular weight, MS/MS count (number of fragmentation spectra for each protein)
4. T-test p-value
5. The corrected t-value considering the repeated tests (False Discovery Rate, FDR)
6. The Quantitative difference of the abundance of each protein in the compared conditions (BBS10 - CTRL)

The putativeBBS10 interactors were selected among the significant proteins from supplementary **Table S3**, being more abundant in BBS10 interactome with respect to GFP non-specific interactome. To estimate the BBS10-flag abundance compared to the endogenous protein, the amount of protein was measured in total extracts from HEK293T_BBS10 and wt HEK293T (HEK293T_CTRL) cell lines by mass-spectrometry-based quantitative methods. The protein abundance was estimated by

using normalized MS counts (**Table S4**), as the ratio between the MS counts of the interest proteins and the total MS counts in the analyzed sample.

After, the list of interactors was subjected to clusterization using STRING (Search Tool for the Retrieval of Interacting Genes) online version 11, in order to evaluate the mitochondrial proteins into dataset. The cluster was evaluated by a significant interaction score as negative logarithm of the p-value.

Western Blot

Protein sample were fractionated by a 10% SDS-PAGE, and transferred onto nitrocellulose membranes using a Trans-Blot Turbo Transfer System (Bio-Rad, Hercules, CA, USA). Membranes were blocked for 2 h at room temperature with 5% milk in PBS with a 0.2 % Tween-20. Each primary antibody used for WB was incubated O/N at 4 ◦C in 5% milk in PBS with a 0.2 % Tween-20.

All antibodies used in this study are commercially available and are listed below. From Abcam: Citrate synthase (ab96600, Abcam). From Sigma-Aldrich: α-tubulin (T6074) and Flag M2 (F1804). From Millipore: Vdac1 (AB10527).

Immunoblot detections were carried out using horseradish peroxidase-conjugated antibodies (Claritry Western ECL Substrate, Biorad, USA) and enhanced chemiluminescence (Claritry Max Western ECL Substrate, Biorad, USA). Signals were acquired by Biorad Chemidoc. Densitometry analysis was performed by ImageJ Fiji software.

Quantitative Real-Time PCR

For each qRT-PCR assay, 1.5×10^3 cells/mm2 of mIMCD3 cells were seeded in a 6 cm diameter plate and kept in culture in standard conditions (see above). After 24 h, cells were washed twice with PBS and total RNA was extracted from kidney cells using EUROGOLD TriFast reagent (EuroClone, Paington, UK). 500 ng of RNA were reverse-transcribed using SuperScript™ VILO™ MasterMix (Thermo Fisher Scientific, Bremen, Germany). Then, qRT-PCR was carried out in a 7900 Real-Time PCR System PCR Thermal Cycler with appropriate primers using a SYBR® Select Master Mix (Applied Biosystems, Monza, Italy). Gene expression levels of Bbs10, PPAR-α, PPAR-γ, PGC1a Acox1, Cpt1 and Cpt2, were normalized to RNA polymerase II (Polr2A) and β2 microglobulin protein and calculated using the $2^{-\Delta Ct}$ method. Average values from at least three independent experiments were graphically reported as relative units. Statistical significance was calculated by a two-tail unpaired t-test. The primers sequences are reported below.

Primers	Forward 5'- 3'	Reverse 5'-3'
β2 Microglobulin	GGT CTTTCTGGTGCTTGTTCT	TATGTTCGGCTTCCCATTCTC
Polr2a	GGATGAATTGAAGCGGATGTC	CACTCGGTCATGTTTCCTGC

Bbs10	CAAGTGTTGTGTACGAAGCC	CACACGCCACTATCATCCTG
PPAR-α	TGCAAACTTGGACTTGAACG	GATCAGCATCCCGTCTTTGT
PPAR-γ	AGGATGCAAGGGTTTTTTCCG	ACCTGATGGCATTGTGAGAC
Cpt1	GGTCTTCTCGGGTCGAAAGC	TCCTCCCACCAGTCACTCAC
Cpt2	CAATGAGGAAACCCTGAGGA	GATCCTTCATCGGGAAGTCA
Acox1	CTTGGATGGTAGTCCGGAGA	TGGCTTCGAGTGAGGAAGTT
PGC1a	AGTCCCATACACAACCGCAG	CCCTTGGGGTCATTTGGTGA

Mitochondrial protein extracts

Mitochondrial extracts were obtained as elsewhere described (Clayton and Shadel, 2014). Briefly, 60 million cells, were washed twice in PBS and harvested by scraping in PBS. The cell suspension was than centrifuged at 230 RCF for 10 minutes at 4°C and the cell pellet was resuspended in 2.2 mL of RSB hypotonic buffer (10 mM NaCl, 1.5 mM $MgCl_2$, 10 mM Tris-HCl pH 7.5, protease inhibitor cocktail) and incubated at 4°C for 15 minutes. The cell suspension was then put into a Dounce homogenizer and at least 5 strokes were applied. The homogenate was then trasferred into a clean tube and 1.6 mL of 2.5X MS homogenization buffer (525 mM mannitol, 175 mM sucrose, 12,5 mM Tris-HCl pH 7.5, 2.5 mM EDTA, protease inhibitor cocktail) were added. The homogenate was then centrifuged at 1,300 RCF for 5 minutes at 4°C and the supernatant was recovered and put into a clean tube. This tube was again centrifuged at 1,300 RCF for 5 minutes at 4°C and the supernatant was again put into a clean tube. This last procedure (centrifugation and supernatant recovery) was performed one more time and the supernatant was then centrifuged at 17,000 RCF for 15 minutes at 4°C. The supernatant was discarded and the pellet of mitochondria was resuspended in 1X MS homogenization buffer (210 mM mannitol, 70 mM sucrose, 5 mM Tris-HCl pH 7.5, 1 mM EDTA, protease inhibitor cocktail). The suspension was again centrifuged at 17,000 RCF for 15 minutes at 4°C and the supernatant was discarded. The pellet of mitochondria was resuspended in RIPA buffer (25 mM Tris-HCl pH 7.5, 150 mM NaCl, 1% Triton X-100, 1% sodium deoxycholate, 0.1% SDS, 1 mM EDTA, protease inhibitor cocktail) and incubated for 20 minutes at 4°C under shaking. This last homogenate constituted the mitochondrial extract and was stored at -80°C.

Nucleus-Cytosol subcellular fractionation

Fractioned protein extracts containing cytosolic and nuclear proteins, respectively, were obtained using Qproteome nuclear protein kit (Qiagen Italia, Milan, Italy) as elsewhere described (Fioretti et al., 2021) Briefly, 20 millions cells were washed with PBS, harvested and then centrifuged for 5 min at 450 RCF. Then, they were lysed in 500 µL of hypotonic Buffer NL containing protease inhibitor solution and 0.1 M DTT. Detergent solution was added and, after a shaking, the suspension was centrifuged for 5 min at 10,000 RCF. The supernatant, containing the cytosolic proteins, was

recovered and stored at -80°C. The pellet, containing the cell nuclei, was resuspended in 500 µL of Buffer NL and centrifuged again for 5 min at 10,000 RCF. The nuclear pellet was then resuspended in 50 µL of Buffer NX1 supplemented with protease inhibitor solution and incubated for 30 min under shaking. The suspension was then centrifuged for 10 min at 12,000 RCF and the supernatant was recovered and constituted the first nuclear fraction (N1) containing the nucleic-acid–binding proteins. The pellet was resuspended in 100 µL Buffer NX2 supplemented with benzonase nuclease, protease inhibitor solution and 0.1 M DTT. The suspension was incubated for 1 h under shaking and centrifuged for 10 min at 12,000 RCF. The supernatant was recovered and constituted the second nuclear fraction (N2), containing the insoluble nuclear proteins. To obtain a complete nuclear extract, the two nuclear fractions N1 and N2 were pooled together and stored at -80°C. The Qproteome® Nuclear Protein Kit provided all the aforementioned buffer solutions and reagents and all the steps of the procedure were performed at 4°C.

Quantification and statistical analysis

Statistical analyses were performed using R software. The serum metabolome dataset was first filtered eliminating metabolites with more than 10 missing data. Subjects with BMI greater than 50 or less than 22 were excluded because the extreme body weights were accompanied by an alteration of the metabolic profile. Values with zero concentration have been replaced by the minimum positive value in the dataset of the same metabolite. The data were then $\log_2$ -transformed and scaled according to the Pareto scaling method. Creatinine was excluded from the analysis as it was used to calculate the eGFR and categorize subjects. The CKD state was coded as 0 if eGFR>90 and 1 otherwise. The Sparse Partial Least Squares Discriminant Analysis (SPLS-DA) in the mixOmics library was then performed separately on BBS subjects and non-BBS subjects, using the CKD state as factor. SPLS-DA is a supervised analysis focusing on the discrimination of the CKD states, thus allowing for relevant feature selection and graphical displays for metabolomic data. The SPLS-DA output performance was tested using the receiver operating characteristic (ROC) curves. Subsequently we computed the influence on the CKD categorization of every metabolite, retrieving the Variable Importance in Projection (VIP). VIP coefficients represent the importance of each metabolite to predict the CKD state. Metabolites with VIP score greater than 1 were then used for subsequent analysis. Therefore, two lists of metabolites with VIP score>1 were obtained, one for BBS patients and one for non-BBS patients. The two lists were then compared and only the metabolites present exclusively in BBS patients were then evaluated.

The resulting metabolites BBS-specific were then confirmed testing their correlation with the eGFR. To this aim, we used a linear mixed model with the eGFR as dependent variable and as predictors the

metabolite concentration, the genotype (BBS vs non_BBS) and their interaction. Furthermore, the Pearson correlation coefficient between each metabolite and the eGFR was calculated for BBS and non-BBS populations. The differences between BBS and non-BBS regarding the calculated Pearson coefficients were tested using Fisher's r-to-z comparison. Significance level was set at $p<0.05$. Values for continuous variables are expressed as mean±SEM.

Supplementary tables:

Supplementary table 1. Metabolites overview, related to STAR Methods and Results
Supplementary table 2. Serum metabolites concentration (µM), related to STAR Methods and Results
Supplementary table 3. List of selected interactors purified by immunoprecipitation (BBS10-flag and GFP-flag). FDR: false discovery rate (adjustment for repeated t-tests), related to STAR Methods and Results
Supplementary table S4. Details of mass spectrometry protein identification from total protein extract of HEK293T_BB10 and HEK293T wt, related to STAR Methods and Results

Author contributions

EM, MC, DV, AC and NG performed the experiments. MZ designed the experiments and collected the data from human subjects. GC coordinated the in vitro and in vivo experiments. MR and MC analyzed and validated metabolomics studies. VDI, FS, LD, ST recruited patients. DV performed statistical analysis. AC and RF assisted in vitro studies. FDVB and VN performed genetic analysis. All authors participated in the drafting and critical review of the manuscript.

Acknowledgments

This work is generated within the European Reference Network for Rare Kidney Diseases (ERKNet). We acknowledge the Italian Association of BBS patients' families (ASBBI) for its support. We acknowledge Alessia Romano of the Ceinge the Advanced Light Microscopy (ALM) Facility for expert help in data acquisition.

Declaration of interests

The authors declare no competing interests.

Inclusion and diversity

We support inclusive, diverse and equitable conduct of research.

References

BEALES, P. L., ELCIOGLU, N., WOOLF, A. S., PARKER, D. & FLINTER, F. A. 1999. New criteria for improved diagnosis of Bardet-Biedl syndrome: results of a population survey. *J Med Genet,* 36**,** 437-46.

BHATIA, D., CAPILI, A. & CHOI, M. E. 2020. Mitochondrial dysfunction in kidney injury, inflammation, and disease: Potential therapeutic approaches. *Kidney Res Clin Pract,* 39**,** 244-258.

CATERINO, M., ASPESI, A., PAVESI, E., IMPERLINI, E., PAGNOZZI, D., INGENITO, L., SANTORO, C., DIANZANI, I. & RUOPPOLO, M. 2014. Analysis of the interactome of ribosomal protein S19 mutants. *Proteomics,* 14**,** 2286-96.

CATERINO, M., GELZO, M., SOL, S., FEDELE, R., ANNUNZIATA, A., CALABRESE, C., FIORENTINO, G., D'ABBRACCIO, M., DELL'ISOLA, C., FUSCO, F. M., PARRELLA, R., FABBROCINI, G., GENTILE, I., ANDOLFO, I., CAPASSO, M., COSTANZO, M., DANIELE, A., MARCHESE, E., POLITO, R., RUSSO, R., MISSERO, C., RUOPPOLO, M. & CASTALDO, G. 2021. Dysregulation of lipid metabolism and pathological inflammation in patients with COVID-19. *Sci Rep,* 11**,** 2941.

CATERINO, M., ZACCHIA, M., COSTANZO, M., BRUNO, G., ARCANIOLO, D., TREPICCIONE, F., SICILIANO, R. A., MAZZEO, M. F., RUOPPOLO, M. & CAPASSO, G. 2018. Urine Proteomics Revealed a Significant Correlation Between Urine-Fibronectin Abundance and Estimated-GFR Decline in Patients with Bardet-Biedl Syndrome. *Kidney Blood Press Res,* 43**,** 389-405.

CHO, K. H., KIM, H. J., KAMANNA, V. S. & VAZIRI, N. D. 2010. Niacin improves renal lipid metabolism and slows progression in chronic kidney disease. *Biochim Biophys Acta,* 1800**,** 6-15.

CLAYTON, D. A. & SHADEL, G. S. 2014. Isolation of mitochondria from tissue culture cells. *Cold Spring Harb Protoc,* 2014**,** pdb.prot080002.

COSTANZO, M., CATERINO, M., CEVENINI, A., JUNG, V., CHHUON, C., LIPECKA, J., FEDELE, R., GUERRERA, I. C. & RUOPPOLO, M. 2020a. Dataset of a comparative proteomics experiment in a methylmalonyl-CoA mutase knockout HEK 293 cell model. *Data Brief,* 33**,** 106453.

COSTANZO, M., CATERINO, M., CEVENINI, A., JUNG, V., CHHUON, C., LIPECKA, J., FEDELE, R., GUERRERA, I. C. & RUOPPOLO, M. 2020b. Proteomics Reveals that Methylmalonyl-CoA Mutase Modulates Cell Architecture and Increases Susceptibility to Stress. *Int J Mol Sci,* 21.

COSTANZO, M., CEVENINI, A., MARCHESE, E., IMPERLINI, E., RAIA, M., DEL VECCHIO, L., CATERINO, M. & RUOPPOLO, M. 2018. Label-Free Quantitative Proteomics in a Methylmalonyl-CoA Mutase-Silenced Neuroblastoma Cell Line. *Int J Mol Sci,* 19.

COSTANZO, M., ZACCHIA, M., BRUNO, G., CRISCI, D., CATERINO, M. & RUOPPOLO, M. 2017. Integration of Proteomics and Metabolomics in Exploring Genetic and Rare Metabolic Diseases. *Kidney Dis (Basel),* 3**,** 66-77.

FIORETTI, T., CEVENINI, A., ZANOBIO, M., RAIA, M., SARNATARO, D., CATTANEO, F., AMMENDOLA, R. & ESPOSITO, G. 2021. Nuclear FGFR2 Interacts with the MLL-AF4 Oncogenic Chimera and Positively Regulates. *Int J Mol Sci,* 22.

IMPERLINI, E., SANTORELLI, L., ORRU, S., SCOLAMIERO, E., RUOPPOLO, M. & CATERINO, M. 2016. Mass Spectrometry-Based Metabolomic and Proteomic Strategies in Organic Acidemias. *Biomed Res Int,* 2016**,** 9210408.

LEVEY, A. S., STEVENS, L. A., SCHMID, C. H., ZHANG, Y. L., CASTRO, A. F., 3RD, FELDMAN, H. I., KUSEK, J. W., EGGERS, P., VAN LENTE, F., GREENE, T., CORESH, J. & CKD, E. P. I. 2009. A new equation to estimate glomerular filtration rate. *Ann Intern Med,* 150**,** 604-12.

LIN, J., CHEN, K., CHEN, W., YAO, Y., NI, S., YE, M., ZHUANG, G., HU, M., GAO, J., GAO, C., LIU, Y., YANG, M., ZHANG, Z., ZHANG, X., HUANG, J., CHEN, F., SUN, L., ZHANG, X., YU, S., CHEN, Y., JIANG, Y., WANG, S., YANG, X., LIU, K., ZHOU, H. M., JI, Z., DENG, H., HAQUE, M. E., LI, J., MI, L. Z., LI, Y. & YANG, Y. 2020. Paradoxical Mitophagy Regulation by PINK1 and TUFm. *Mol Cell,* 80**,** 607-620 e12.

LIU, L., ZACCHIA, M., TIAN, X., WAN, L., SAKAMOTO, A., YANAGISAWA, M., ALPERN, R. J. & PREISIG, P. A. 2010. Acid regulation of NaDC-1 requires a functional endothelin B receptor. *Kidney Int,* 78**,** 895-904.

LUCIANI, A., SCHUMANN, A., BERQUEZ, M., CHEN, Z., NIERI, D., FAILLI, M., DEBAIX, H., FESTA, B. P., TOKONAMI, N., RAIMONDI, A., CREMONESI, A., CARRELLA, D., FORNY, P., KOLKER, S., DIOMEDI CAMASSEI, F., DIAZ, F., MORAES, C. T., DI BERNARDO, D., BAUMGARTNER, M. R. & DEVUYST, O.

2020. Impaired mitophagy links mitochondrial disease to epithelial stress in methylmalonyl-CoA mutase deficiency. *Nat Commun,* 11**,** 970.

MARCHESE, E., RUOPPOLO, M., PERNA, A., CAPASSO, G. & ZACCHIA, M. 2020. Exploring Key Challenges of Understanding the Pathogenesis of Kidney Disease in Bardet-Biedl Syndrome. *Kidney Int Rep,* 5**,** 1403-1415.

O'FLANAGAN, C. H. & O'NEILL, C. 2014. PINK1 signalling in cancer biology. *Biochim Biophys Acta,* 1846**,** 590-8.

PERNA, A. F., DI NUNZIO, A., AMORESANO, A., PANE, F., FONTANAROSA, C., PUCCI, P., VIGORITO, C., CIRILLO, G., ZACCHIA, M., TREPICCIONE, F. & INGROSSO, D. 2016. Divergent behavior of hydrogen sulfide pools and of the sulfur metabolite lanthionine, a novel uremic toxin, in dialysis patients. *Biochimie,* 126**,** 97-107.

PERNA, A. F., GLORIEUX, G., ZACCHIA, M., TREPICCIONE, F., CAPOLONGO, G., VIGORITO, C., ANISHCHENKO, E. & INGROSSO, D. 2019. The role of the intestinal microbiota in uremic solute accumulation: a focus on sulfur compounds. *J Nephrol,* 32**,** 733-740.

QU, D., HAGE, A., DON-CAROLIS, K., HUANG, E., JOSELIN, A., SAFARPOUR, F., MARCOGLIESE, P. C., ROUSSEAUX, M. W., HEWITT, S. J., HUANG, T., IM, D. S., CALLAGHAN, S., DEWAR-DARCH, D., FIGEYS, D., SLACK, R. S. & PARK, D. S. 2015. BAG2 Gene-mediated Regulation of PINK1 Protein Is Critical for Mitochondrial Translocation of PARKIN and Neuronal Survival. *J Biol Chem,* 290**,** 30441-52.

REYES, A., MELCHIONDA, L., BURLINA, A., ROBINSON, A. J., GHEZZI, D. & ZEVIANI, M. 2018. Mutations in TIMM50 compromise cell survival in OxPhos-dependent metabolic conditions. *EMBO Mol Med,* 10.

SEO, S., BAYE, L. M., SCHULZ, N. P., BECK, J. S., ZHANG, Q., SLUSARSKI, D. C. & SHEFFIELD, V. C. 2010. BBS6, BBS10, and BBS12 form a complex with CCT/TRiC family chaperonins and mediate BBSome assembly. *Proc Natl Acad Sci U S A,* 107**,** 1488-93.

THONGNAK, L., PONGCHAIDECHA, A. & LUNGKAPHIN, A. 2020. Renal Lipid Metabolism and Lipotoxicity in Diabetes. *Am J Med Sci,* 359**,** 84-99.

VALENTE, E. M., ABOU-SLEIMAN, P. M., CAPUTO, V., MUQIT, M. M., HARVEY, K., GISPERT, S., ALI, Z., DEL TURCO, D., BENTIVOGLIO, A. R., HEALY, D. G., ALBANESE, A., NUSSBAUM, R., GONZALEZ-MALDONADO, R., DELLER, T., SALVI, S., CORTELLI, P., GILKS, W. P., LATCHMAN, D. S., HARVEY, R. J., DALLAPICCOLA, B., AUBURGER, G. & WOOD, N. W. 2004. Hereditary early-onset Parkinson's disease caused by mutations in PINK1. *Science,* 304**,** 1158-60.

XIU, Y. & FIELD, M. S. 2020. The Roles of Mitochondrial Folate Metabolism in Supporting Mitochondrial DNA Synthesis, Oxidative Phosphorylation, and Cellular Function. *Curr Dev Nutr,* 4**,** nzaa153.

ZACCHIA, M., BLANCO, F. D. V., TORELLA, A., RAUCCI, R., BLASIO, G., ONORE, M. E., MARCHESE, E., TREPICCIONE, F., VITAGLIANO, C., IORIO, V. D., ALESSANDRA, P., SIMONELLI, F., NIGRO, V., CAPASSO, G. & VIGGIANO, D. 2021a. Urine concentrating defect as presenting sign of progressive renal failure in Bardet-Biedl syndrome patients. *Clin Kidney J,* 14**,** 1545-1551.

ZACCHIA, M., BLANCO, F. D. V., TREPICCIONE, F., BLASIO, G., TORELLA, A., MELLUSO, A., CAPOLONGO, G., POLLASTRO, R. M., PILUSO, G., DI IORIO, V., SIMONELLI, F., VIGGIANO, D., PERNA, A., NIGRO, V. & CAPASSO, G. 2021b. Nephroplex: a kidney-focused NGS panel highlights the challenges of PKD1 sequencing and identifies a founder BBS4 mutation. *J Nephrol*.

ZACCHIA, M., CAPOLONGO, G., RINALDI, L. & CAPASSO, G. 2018. The importance of the thick ascending limb of Henle's loop in renal physiology and pathophysiology. *Int J Nephrol Renovasc Dis,* 11**,** 81-92.

ZACCHIA, M., CAPOLONGO, G., TREPICCIONE, F. & MARION, V. 2017. Impact of Local and Systemic Factors on Kidney Dysfunction in Bardet-Biedl Syndrome. *Kidney Blood Press Res,* 42**,** 784-793.

ZACCHIA, M., MARCHESE, E., TRANI, E. M., CATERINO, M., CAPOLONGO, G., PERNA, A., RUOPPOLO, M. & CAPASSO, G. 2020. Proteomics and metabolomics studies exploring the pathophysiology of renal dysfunction in autosomal dominant polycystic kidney disease and other ciliopathies. *Nephrol Dial Transplant,* 35**,** 1853-1861.

ZACCHIA, M., ZACCHIA, E., ZONA, E., CAPOLONGO, G., RAIOLA, I., RINALDI, L., TREPICCIONE, F., INGROSSO, D., PERNA, A., DI IORIO, V., SIMONELLI, F., MOE, O. W. & CAPASSO, G. 2016. Renal phenotype in Bardet-Biedl syndrome: a combined defect of urinary concentration and dilution is associated with defective urinary AQP2 and UMOD excretion. *Am J Physiol Renal Physiol,* 311**,** F686-F694.

ZAGHLOUL, N. A. & KATSANIS, N. 2009. Mechanistic insights into Bardet-Biedl syndrome, a model ciliopathy. *J Clin Invest,* 119**,** 428-37.

Table 1. General characteristics of BBS patients and controls

Parameter	BBS Patients	Controls	p_value
Max u-Osm (mOsm/kgH_20)	580±198	527±205	0.37
BMI (kg/m^2)	32±7	29±7	0.09
Age(years)	29±9	34±8	0.06
eGFR(ml/min/1.73m^2)	80±37	74±35	0.53
n	29	30	-

Table 2. Genetics features of patients' cohort. "No mutations in BBS genes" indicates that the BBS phenotype was due to alterations in unknown genes not belonging to the BBS gene family

Patient ID	Gene	Chr (hg.19)	Genetic mutation	Protein variation	Zygosity
P1	*BBS1*	Chr 11: 66287160	c.664 G>C	p.G222R	HOM
P2	*BBS10*	Chr 12: 76742038	c.101 G>C	p.R34P	HOM
P3	*BBS10*	Chr 12: 76742038	c.101 G>C	p.R34P	HOM
P4	*No mutations in BBS genes*				
P5	*BBS12*	Chr 4: 123665070	c.C2023T/c.C2023T	p.R675X/p.R675X	HOM
P6	*BBS10*	Chr 12: 76740674	c.1091del	p.N364Tfs*5	HOM
P7	*No mutations in BBS genes*				
P8	*BBS10*	Chr 12: 76742038	c.101 G>C	p.R34P	HOM
P9	*No mutations in BBS genes*				
P10	*No mutations in BBS genes*				
P11	*BBS10*	Chr 12: 76741124	c.641T>A	p.V214E	HOM
P12	*BBS4*	Chr 15: 73007751; Chr 15: 73009123	c.332+8T>C c.338delT	spl p.L113fs	DOUBLE HET
P13	*BBS4*	Chr 15: 73007744	c.332+1G>GTT	spl	HOM
P14	*BBS4*	Chr 15: 73007744	c.332+1G>GTT	spl	HOM
P15	*BBS2*	Chr 16: 56530878	c.1909_1910del	p.M637Efs* 12	HOM
P16	*BBS1*	Chr 11: 66287160	c.664G>C	p.G222R	HOM
P17	*BBS9*	Chr 7: 33296990 Chr 7: 33545112	c.585_586del c.2033delG	p.V196LFs*10 G678Afs*10	DOUBLE HET
P18	*BBS1*	Chr 11: 66293652	c.1169T>G c.1642delC	p.M390R p. L548Wfs*31	DOUBLE HET

		Chr 11: 66299160			
P19	*BBS10*	Chr 12: 76741436 Chr 12: 76741994	c.325_328del c.145C>T	p.M109Vfs*25	DOUBLE HET
P20	*No mutations in BBS genes*				
P21	*No mutations in BBS genes*				
P22	*BBS9*	Chr 7: 33185869 Chr 7: 33384190	c.6_6delT c.1276-1277delAGCA	p.L3Yfs*38 p.Q426Sfs*5	DOUBLE HET
P23	*BBS12*	Chr 4: 123665070	c.2023C>T	p.R675X	HOM
P24	*BBS12*	Chr 4: 123665070	c.2023C>T	p.R675X	HOM
P25	*BBS4*	Chr 15: 73007744 Chr 15: 73027508	c.332+1G>GTT c.1091C>A	spl	DOUBLE HET
P26	*No mutations in BBS genes*				
P27	*BBS9*	Chr 7: 33312706	c.T785C	p.V262A	HOM
P28	*BBS9*	Chr 7: 33296989 Chr 7: 33185912	c.586_587del c.51_54del	p.VaI196Leufs*10 p.Glu18Asnfs*22	DOUBLE HET
P29	*BBS9*	Chr 7: 33296989 Chr 7: 33185912	c.586_587del c.51_54del	p.VaI196Leufs*10 p.Glu18Asnfs*22	DOUBLE HET

Table.3 Statistical analysis of BBS specific metabolites correlated to eGFR.

	Pearson coefficient metabolite x eGFR (p)			VIP		Lm (eGFR = genetic + metabolite + genetic*metabolite)		
Metabolite	**BBS**	**Controls**	**Pearson BBS vs Pearson controls (p)**	**BBS**	**Controls**	**BBS effect (p)**	**eGFR effect (p)**	**BBS x metabolite interaction effect (p)**
C10:1	-0.69 (<0.01)	-0.30 (>0.05)	0.05	2.04	0.45	0.97	0.00	0.04
C14:2-OH	-0.55 (<0.01)	0.00 (>0.05)	0.02	1.61	0.74	0.69	0.02	0.03
C16:1	-0.70 (<0.01)	-0.25 (>0.05)	0.02	2.16	0.23	0.86	0.00	0.02
lysoPC a C26:0	0.63 (<0.01)	0.10 (>0.05)	0.02	2.05	0.09	0.00	0.00	0.03
PC aa C24:0	0.52 (<0.01)	-0.25 (>0.05)	0.00	1.54	0.14	0.93	1.00	0.02
PC aa C26:0	0.55 (<0.01)	0.02 (>0.05)	0.03	2.09	0.11	0.00	0.02	0.05
PC aa C32:0	-0.58 (<0.01)	-0.08 (>0.05)	0.03	1.47	0.56	0.23	0.01	0.08
PC aa C32:3	-0.61 (<0.01)	0.08 (>0.05)	0.00	1.33	0.65	0.32	0.06	0.02
PC aa C42:5	-0.58 (<0.01)	-0.05 (>0.05)	0.02	1.36	0.06	0.46	0.01	0.06
PC ae C42:1	-0.46 (<0.01)	0.11 (>0.05)	0.03	1.40	1.05	0.58	0.15	0.04

VIP: variable importance in the projection, Lm: linear model formula

Table 4. BBS10 mitochondrial interactors

Gene ID	Protein ID	Function
BAG2	O95816	Regulate mitochondrial clearance through recruitment of PARKIN by stabilization of PINK1 on the outer membrane of depolarized mitochondria. Bcl2-associated athanogene 2 (BAG2) as a factor that promotes mitophagy and physically interact with PINK1 (Qu et al., 2015)
TUFM	P49411	Homeostasis of pink1/parkin-dependent mitophagy regulation (Lin et al., 2020)
MTHFD1L	Q6UB35	folate-mediated one-carbon (1C) metabolism pathway (Xiu and Field, 2020)
ACAT1	P24752	As mitochondrial acetoacetyl-CoA thiolase is involved in beta-oxidation. The deficiency in this enzyme is associated with an increased amount of cholesterol compounds. Its deregulation in CKD is associated to lipids accumulation (Cho et al., 2010)
GOT2	P00505	Facilitates cellular uptake of long-chain free fatty acids
TIMM50	Q3ZCQ8	TIMM50 is an essential component of the TIM23 complex, the mitochondrial inner membrane machinery that imports cytosolic proteins into the mitochondrial inner compartment. TIMM50 is essential for cell survival in OxPhos-dependent conditions (Reyes et al., 2018)

Legend of figures

Figure 1. Partial least squares-discriminant analyses (PLS-DA) and ROC curve of serum metabolome showed discrimination of the CKD status in BBS patients (n=29) and controls(n=30). A-B: plot of the first two PLS-DA components discriminating subjects according to CKD status in the control group (A: controls, B: BBS). C-D: Receiver Operating Characteristic (ROC) curve are presented to evaluate performances and robustness of the PLS-DA model. The AUC was high in both control (C, AUC = 0.99) and BBS patients (D, AUC = 0.94). E-F: the relevance of each metabolite for the discrimination of the CKD status was indexed by the variable importance in the projection (VIP) scores. A VIP score less than 1 indicates that the variable is not important for the discrimination. Only variables with VIP scores>1.5 are reported for graphical reasons.

Figure 2. Determination of BBS specific metabolites associated to eGFR decline. A: Venn diagram of metabolites discriminating the CKD status in the BBS **(n=29)** and control(**n=30**) populations based on a VIP score>1. The intersection between the two sets is also reported. B. BBS specific metabolites were further filtered as follows: (i) not included in the list of control VIP metabolites (ii) significant correlation with eGFR (iii) and significant difference between BBS and controls regarding the calculated Pearson coefficient. The scatterplot of the eGFR vs the resulting 10 metabolites is presented.

Figure 3. **Generation of stable renal tubular epithelial cell line lacking Bbs10 gene (IMCD3-*Bbs10*-/-). A**: microscopy images of CRISPR/Cas9-modified cells. After transfection, cells were observed with a 20× objective and images were acquired with the Leica LAS AF software. mIMCD3 Bbs10-/- clone: Cell populations isolated from single progenitor cells within the Bbs10-/- pool. RFP: Fluorescence signal from the red fluorescent protein detected with a Leica N3 filter cube. To limit clone dependent effects, four different KO clone cells were used, in addition to the negative control line transfected with Cas Nuclease Only **B**: real-time analysis of Bbs10 gene expression level in Bbs10 -/- cells and wild type cells. Relative mRNA expressions of Bbs10 in mIMCD3 Bbs10-/- cells (n=20) and wild type cells (n=5). Data are presented as mean ± SEM, are normalized to wild type controls as y-axis is indicated by % fold The statistical significance of the difference in mRNA expressions between conditions (mIMCD3 Bbs10-/- cells and wild type controls) was evaluated by unpaired parametric t test with Welch correction **C**: number of primary cilia in mIMCD3-Bbs10-/- cells (n=) compared to wild type cells. Immunofluorescence staining of 24- and 48-hours' serum starved cells (wild type vs Bbs10-/- cells) with antibodies against Arl13b (primary cilium, red), γ- tubulin (basal body, green) and DAPI (DNA, blue in merge). Magnifications area shown in white boxes, white scale bars 5 μm **D**: significant differences in the number of cilium presenting cells were observed, with a decrease of ciliated cells in Bbs10 -/- condition both at 24 and 48 hours of serum starvation ($p < 0.05$ [χ2-test], white scale bars 10 μm). **E:** Bbs10-/- cells (n=18) showed a significantly increased mitotic rate compared with wild type cells (n=7) (*p<0.05, **p<0.01, *** p<0.001****p<0.0001, ns = not significant)

Figure 4. Lipid droplets in IMCD3-Bbs10-/-cells and control. A: Representative images of mIMCD3 kidney tubular cells treated with FFA (1.5nM) for 24 hours. FFA uptake was demonstrated by Oli Red O staining (red). Nuclei were counterstained with Hematoxylin (blue). B: greater magnification of mIMCD3 cells after FFA treatment demonstrating the accumulation of FFA droplets in Bbs10-/- cells. Wild type cells are not shown as they do not accumulate FFA. C. quantification of FFA droplets after treatment. Three independent observers quantified the amount of lipid droplets in the cells giving a score from 0 (no cells with droplets) to 2 (all cells showing droplets). For each condition, the average score among blinded observers was considered. Barplot represents mean±sem of experimental triplicates. Scalebar= 50micron (A), 10micron (B)

Figure 5. Mitochondrial membrane potential and mitochondrial αCS in mIMCD3-*Bbs10* -/- cells. A**:** wild type (n=6) and Bbs10-/- cells (n=18) are stained with mitotracker red CMXros that are sensible to membrane potential (in red) and with citrate synthase fluorescent antibody that marks all mitochondria and is an indicator of mitochondrial biomass (in green) (white scale barr 10 μm, objective 63X). Cells 24 hour after seeding are incubated with medium contained mitotracker red CMXros at final concentration of 200nM for 40 min at 37°C. After incubation, cells are fixed in cold methanol and subjected to immunofluorescence protocol according to Citrate synthase antibody specification. B: Bbs10-/- and wild type Mitochondria's images at higher magnification (white scale bar 5 μm). Mitochondrial images were acquired with the confocal microscope LSM980 with 63X objective (NA 1.63) in Airyscan mode to obtain super-resolution images. C: The analysis of fluorescence was carried out with Zen 3.1 software. The membrane potential results from the ratio between intensity mean value of each channel and the numbers of nuclei stained with Dapi. The data are expresses ad % fold change wt versus Bbs10-/-. The analysis shows significant decrease of membrane potential and of total mitochondria biomass in Bbs10 depleted cells compared to wild type cells. (p value <0.05).

Figure 6. **Proposed model depicting the link between mitochondrial dysfunction and *Bbs10* loss in kidney epithelial cells**. In wild-type kidney cells (left), the PINK1/Parkin-induced mitophagy maintains the quality of the mitochondrial network by priming dysfunctional mitochondria for autophagy–lysosome degradation pathways. BAG2 physically interacts with PINK1 *in vivo* and stabilizes PINK1 from proteasomal degradation, facilitates recruitment of PARKIN to depolarized mitochondria. By contrast, in *Bbs10*-depleted kidney cells (right), the impaired PINK/Parkin-mediated mitophagy reduces the ability to clear from damaged mitochondria, leading to accumulation of diseased mitochondria and collapsed mitochondrial membrane potential ($\Delta\psi m$). The image was created using Biorender (https://biorender.com/)

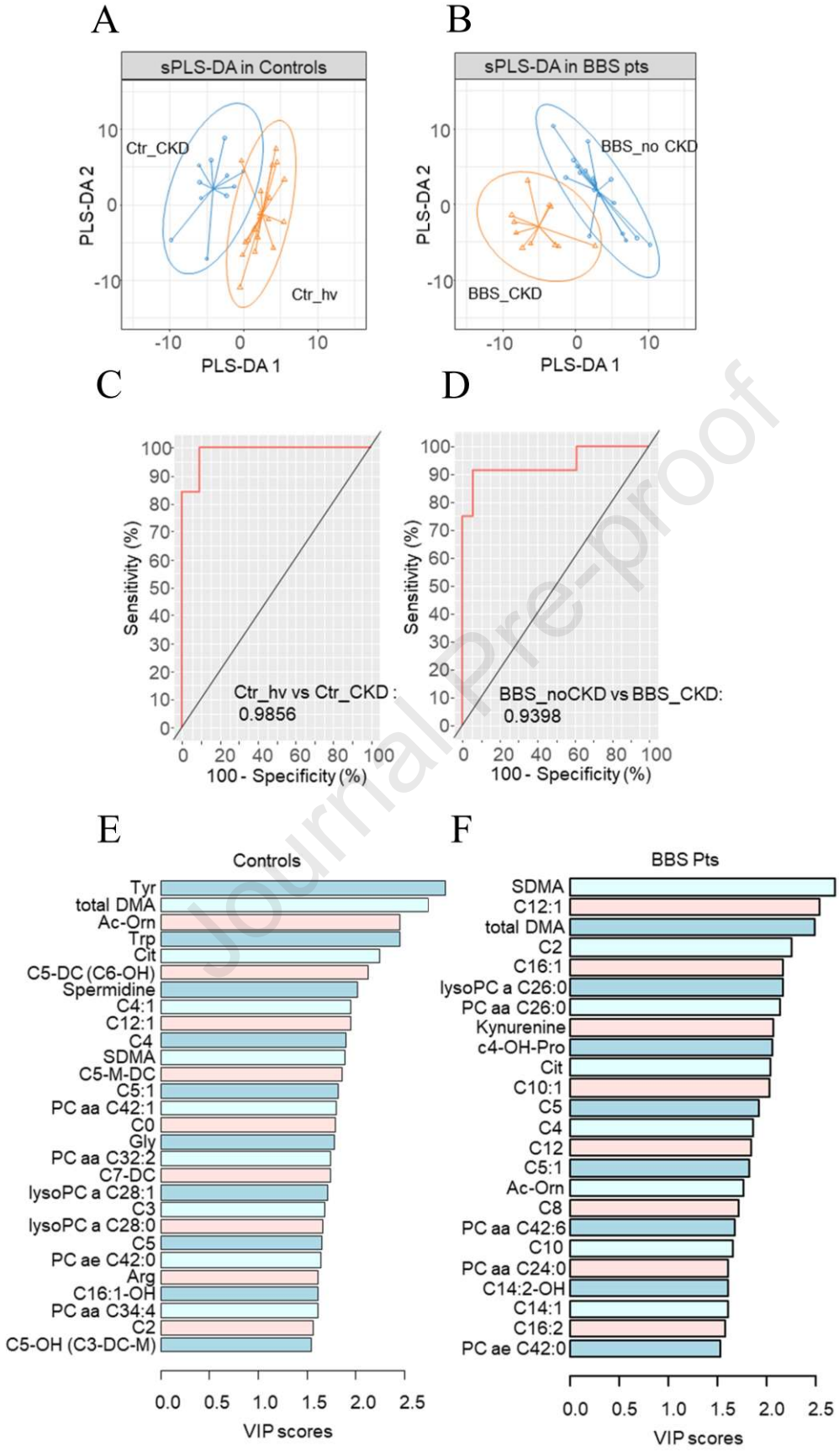

A

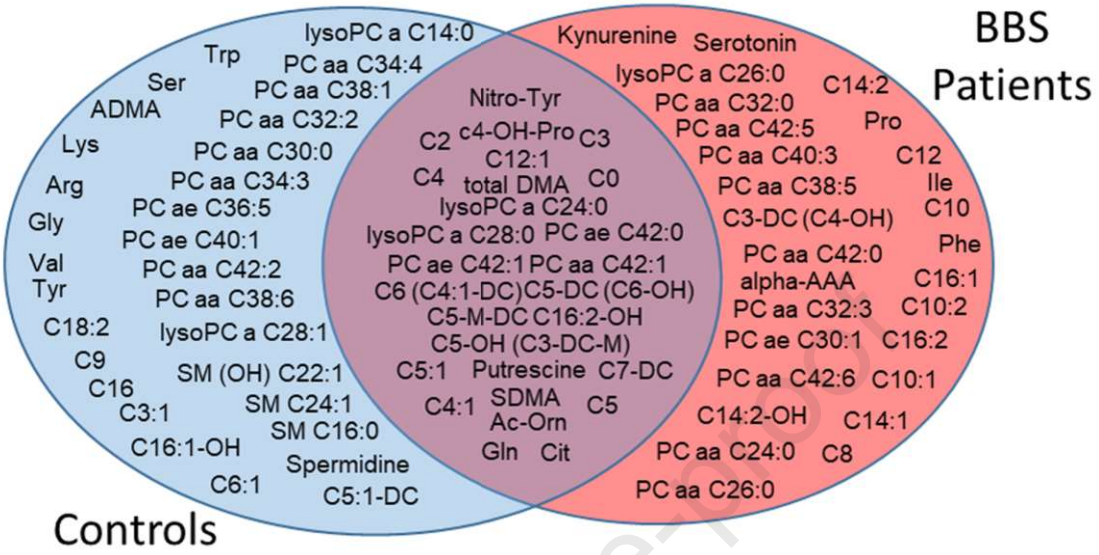
BBS Patients
Controls
lysoPC a C14:0
Trp
PC aa C34:4
Ser
PC aa C38:1
ADMA
PC aa C32:2
Lys
PC aa C30:0
Arg
PC aa C34:3
PC ae C36:5
Gly
PC ae C40:1
Val
PC aa C42:2
Tyr
PC aa C38:6
C18:2
lysoPC a C28:1
C9
C16
SM (OH) C22:1
C3:1
SM C24:1
SM C16:0
C16:1-OH
Spermidine
C6:1
C5:1-DC
Nitro-Tyr
C2
c4-OH-Pro
C3
C12:1
C4
total DMA
C0
lysoPC a C24:0
lysoPC a C28:0
PC ae C42:0
PC ae C42:1
PC aa C42:1
C6 (C4:1-DC)
C5-DC (C6-OH)
C5-M-DC
C16:2-OH
C5-OH (C3-DC-M)
C5:1
Putrescine
C7-DC
C4:1
SDMA
C5
Ac-Orn
Gln
Cit
Kynurenine
Serotonin
lysoPC a C26:0
C14:2
PC aa C32:0
PC aa C42:5
Pro
PC aa C40:3
C12
PC aa C38:5
Ile
C3-DC (C4-OH)
C10
PC aa C42:0
Phe
alpha-AAA
C16:1
PC aa C32:3
C10:2
PC ae C30:1
C16:2
PC aa C42:6
C10:1
C14:2-OH
C14:1
PC aa C24:0
C8
PC aa C26:0

B

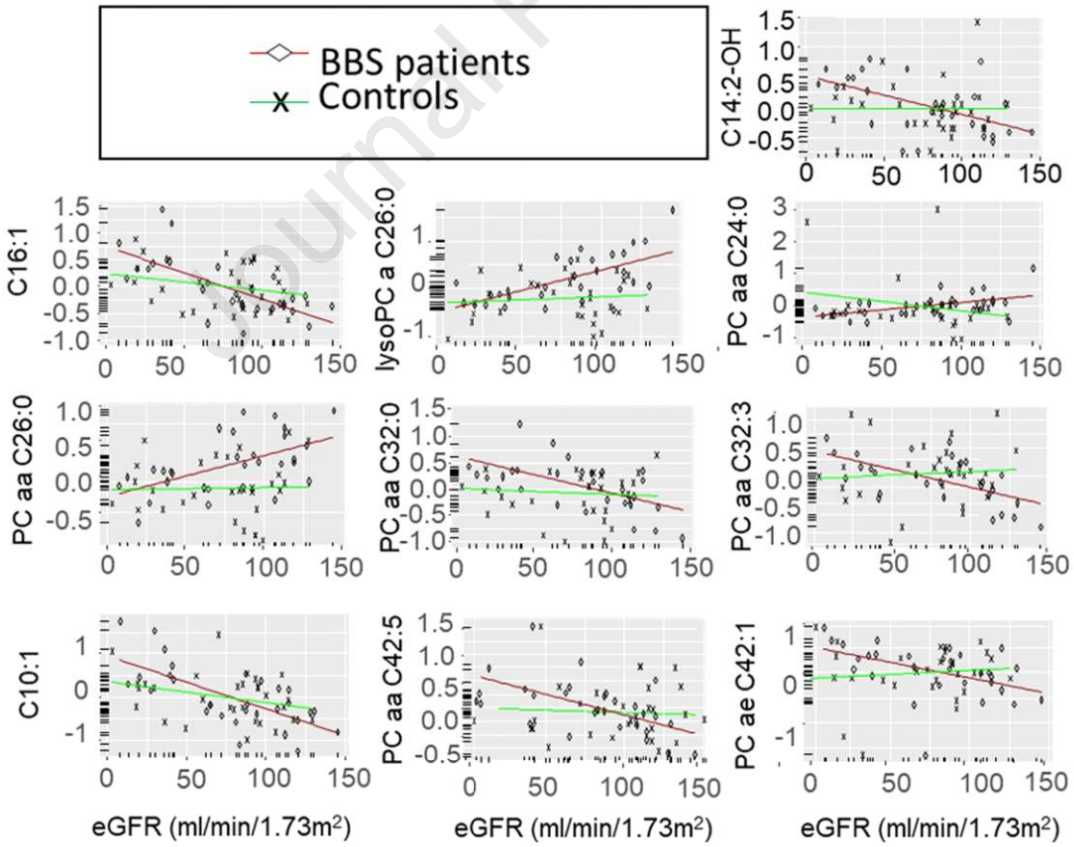
BBS patients
Controls
C14:2-OH
C16:1
lysoPC a C26:0
PC aa C24:0
PC aa C26:0
PC aa C32:0
PC aa C32:3
C10:1
PC aa C42:5
PC ae C42:1
eGFR (ml/min/1.73m²)
eGFR (ml/min/1.73m²)
eGFR (ml/min/1.73m²)

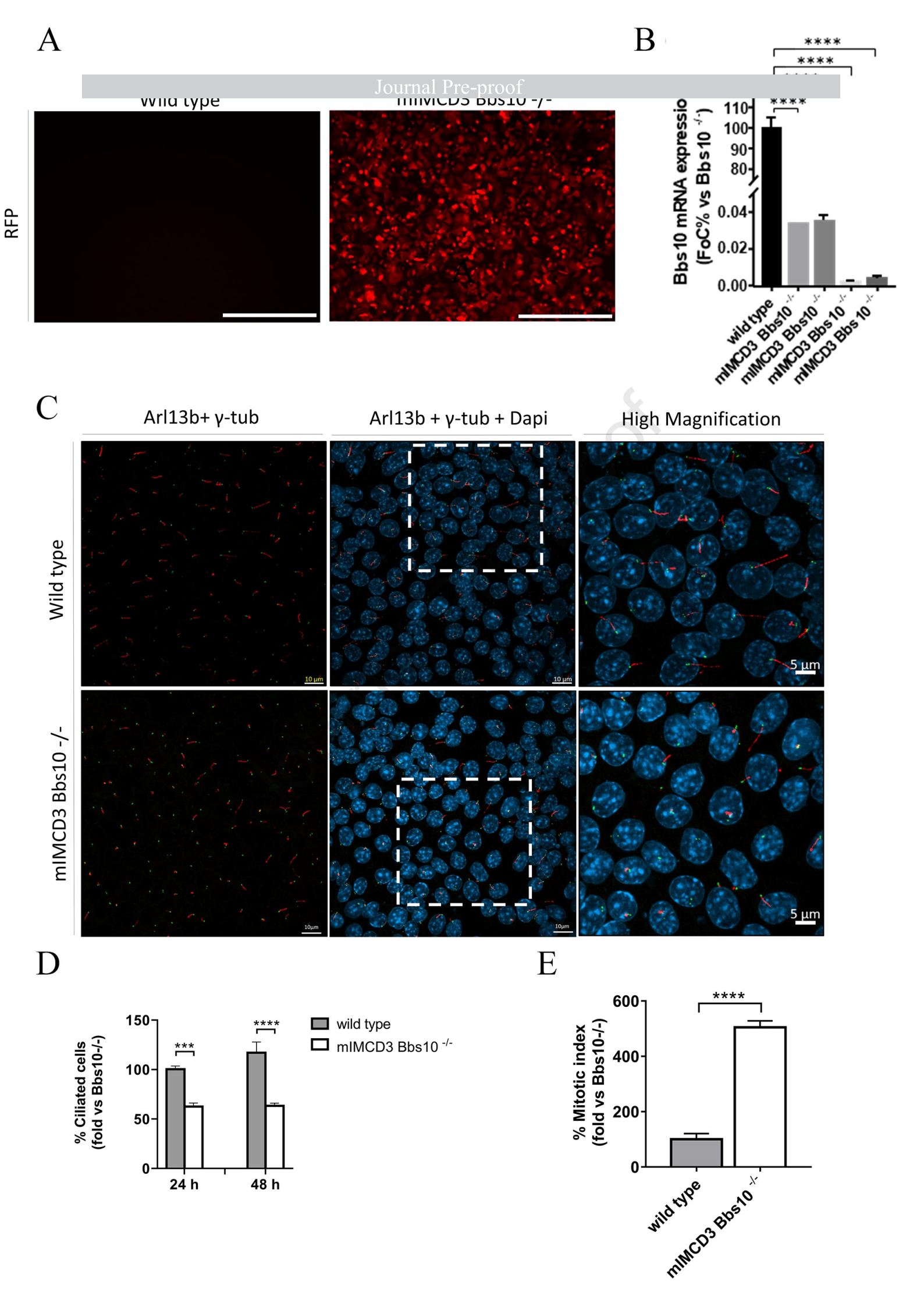

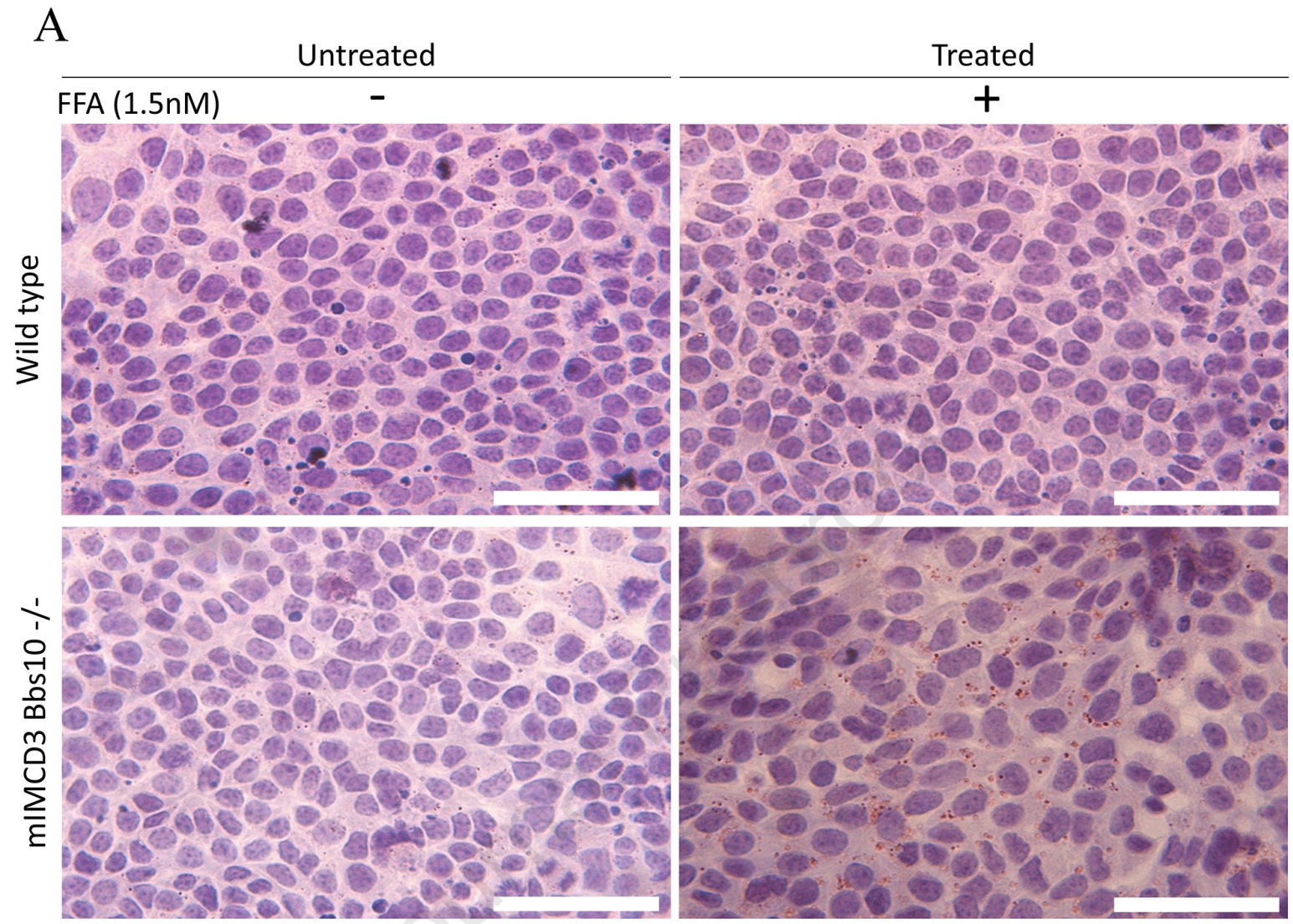
A
Untreated
Treated
FFA (1.5nM)
-
+
Wild type
mIMCD3 Bbs10 -/-

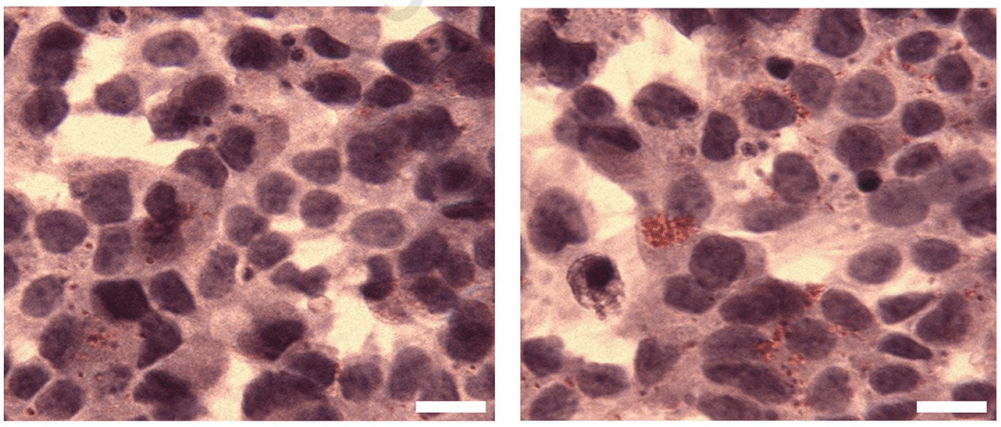
B
mIMCD3 Bbs10-/-
Untreated
mIMCD3 Bbs10-/-
FFA (1.5nM) Treated

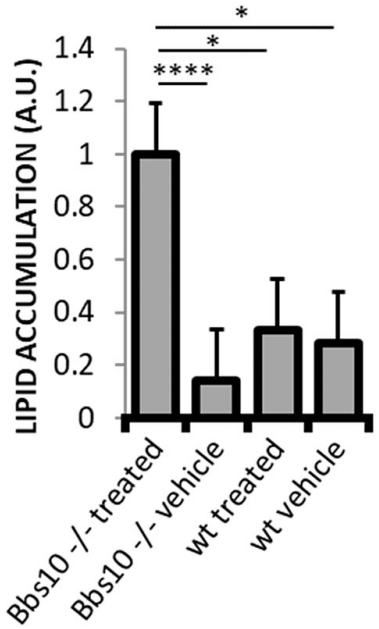
C
LIPID ACCUMULATION (A.U.)
1.4
1.2
1
0.8
0.6
0.4
0.2
0
****
*
*
Bbs10 -/- treated
Bbs10 -/- vehicle
wt treated
wt vehicle

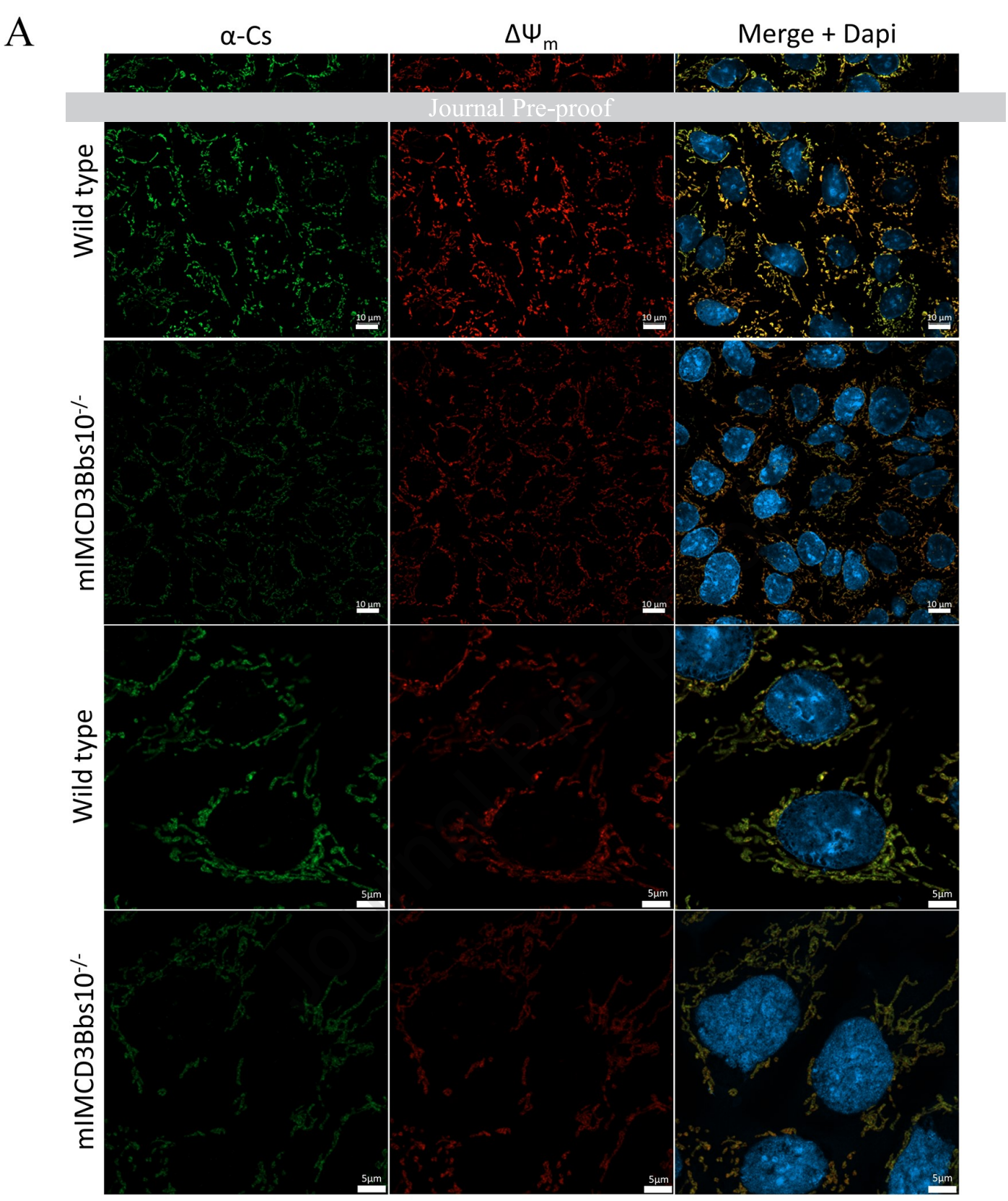

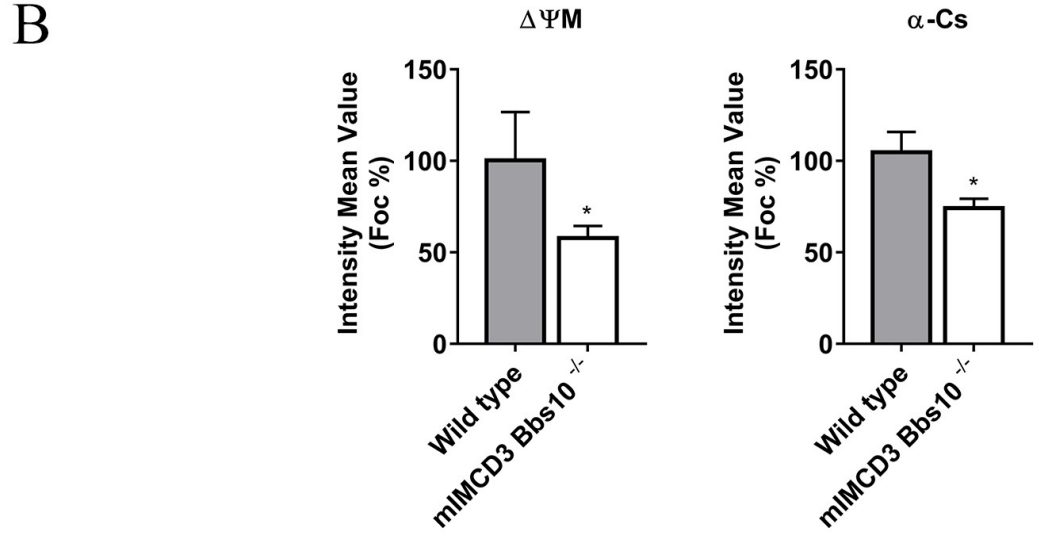

Wild type epithelial renal cell

Bbs10 -/- epithelial renal cell

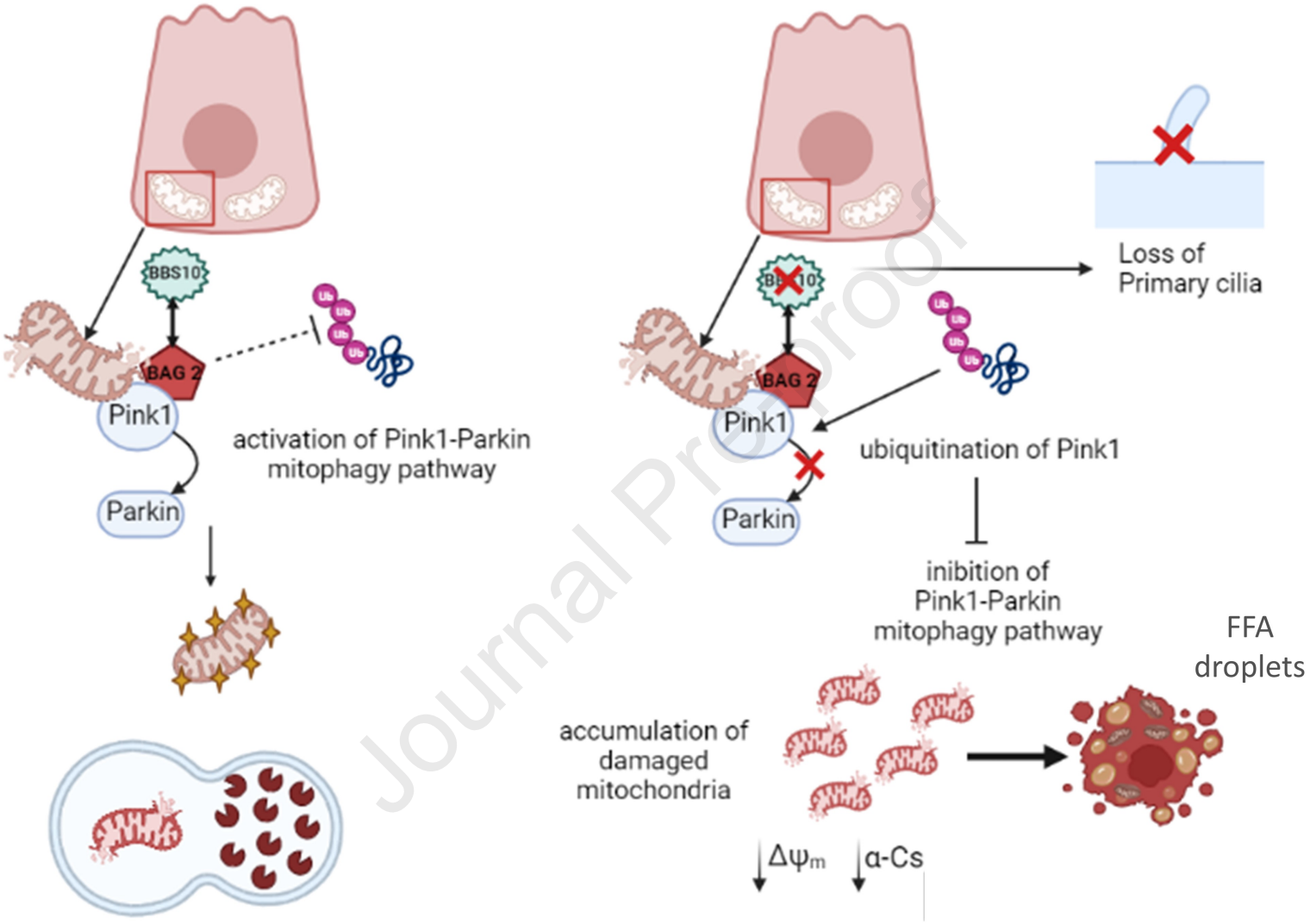

Highlights

- Targeted Metabolomics reveals a unique serum fingerprinting of BBS patients with CKD
- Acylcarnitines are among the most significant alterations
- In renal epithelial cells, *Bbs10* depletion leads to mitochondrial abnormalities
- Human BBS 10 interacts with six mitochondria-related proteins